Nonlinear Dynamic Behaviour and Seismic Fragility Analysis of Irregular Multi-Span RC Bridges

Ebrahim Afsar Dizaj[a*], Mohammad R. Salami[b], Mohammad M. Kashani[c]

[a]Assistant Professor, Department of Civil Engineering, Azarbaijan Shahid Madani University, Tabriz, Iran. (corresponding author), Email: ebrahim.afsardizaj@azaruniv.ac.ir

[b]Senior Lecturer in Civil Engineering, School of Engineering and the Built Environment, Birmingham City University, B5 5JU, United Kingdom, Email: mohammad.salami@bcu.ac.uk

[c]Associate Professor, Faculty of Engineering and Physical Sciences, University of Southampton, Southampton, SO17 1BJ, United Kingdom, Email: mehdi.kashani@soton.ac.uk

Abstract

This paper investigates the nonlinear dynamic behaviour and failure probability of multi-span Reinforced Concrete (RC) bridges supported on piers of unequal heights. To this end, a three-dimensional nonlinear finite element model of RC bridges with substructure irregularity is developed. The model is verified against an available experimental data of a large-scale shake table test results of a benchmark irregular two-span RC bridge. Six hypothetical two-span irregular RC bridges with piers varied in height, and various superstructure mass-distribution conditions (equal and unequal) and a regular bridge layout (as a reference) are considered. Through Incremental Dynamic Analyses (IDAs), the seismic performance of selected bridge layouts is investigated at both local and global scales. Finally, the influence of bridge layout on seismic vulnerability of piers of varying heights is analysed. Results show that the unbalanced seismic displacement demand and failure probability of different bents of a multi-span irregular RC bridge significantly depend on the height of piers and their arrangement. Therefore, the typical

presumption of shorter piers having a higher failure probability due to their higher seismic force absorption is not always the most possible failure mechanism.

Keywords: Irregularity; RC bridge; IDA; Fragility analysis; Reinforced concrete; Modal analysis

1. Introduction

Bridges serve as critical links in any transportation network and have several socio-economic impacts. The closure or disruption of even a single bridge within a transportation network can notably affect economic activities, isolate different communities and cause severe impacts on transportation distances. Therefore, the integrity and adequate safety of bridges should be ensured, particularly after extreme seismic events. Consequently, maintaining the functionality and reliable seismic performance of bridges are of prime importance to stakeholders and bridge owners [1].

Bridges located in mountainous areas or steep-sided river crossings are commonly constructed with piers of unequal heights [2-3]. Due to the aesthetic and practical considerations, piers of such bridges are typically built with identical cross-section dimensions. The resulting substructure stiffness irregularity leads to unbalanced seismic ductility demand of piers, where the shorter piers attract higher seismic demands due to their relatively higher stiffness. This uneven distribution of seismic forces results in a complex seismic response of such bridges, where the accumulation of damage in stiffer members increases the likelihood of brittle failure [4-8]. Concerning such problematic complexities, design codes provide balanced stiffness recommendations to ensure the regular response of multi-span RC bridges [9-10]. It has been notified that not meeting the recommendations above will result in an increased irregular seismic response of the multiple frame bridges. In addition to the code recommendations, several approaches have been proposed in the literature to mitigate the irregular seismic behaviour of multiple frame bridges built on rugged

topography. Reducing the cross-section size, strengthening short piers, using yielding dampers, regulating the reinforcement ratio in piers of varying height, damping and isolation devices at the pier to superstructure connections, and adjusting the pier to deck connection are just examples of such approaches [3,11-14].

The nonlinear seismic performance analysis of RC bridges with irregular configurations has been widely investigated in the literature [15-24]. The outcome of previous studies shows that multi-span RC bridges with substructure irregularity are more vulnerable than regular bridges. Moreover, the vulnerability of irregular RC bridges increases significantly as their altitudinal irregularly increases [25-26]. Gomez-Soberon et al. [24] analysed the seismic performance of several highway bridges with various irregularity conditions. The analyses outputs of [24] showed that the height difference of adjacent piers significantly affects the vulnerability of bridges with substructure irregularity. Soleimani et al. [15] conducted sensitivity analyses on concrete bridges with various irregularities to identify the most influential parameters in the seismic response of irregular RC bridges. The findings of Soleimani et al. [15] indicate that pier diameter, longitudinal reinforcement ratio, earthquake intensity level, pier height, compressive strength of concrete and span length are the most influencing parameters determining the seismic behaviour of irregular RC bridges. Soltanieh et al. [16] investigated the influence of soil-foundation-structure interaction on the seismic vulnerability of irregular RC bridges. They concluded that including the soil-structure interaction in the finite element model of irregular RC bridges considerably affects the distribution of demands in different piers. Hu and Guo [17] studied the seismic response of high-speed railway bridge-track systems with unequal height pier layouts. The results indicated that increasing the height difference of adjacent bridge piers intensifies the seismic displacement responses of sliding layer, shear alveolar and moveable bearings. Jara et al. [19] studied the

influence of soil type on the expected damage of piers in irregular RC bridges. They concluded that while the hard soil ground motion records trigger moderate damage in bridge piers, the soft soil records impose severe damage in piers and cause their failure. Rezaei et al. [27] investigated the effects of ground motion incidence angle on the seismic vulnerability of irregular box-girder concrete bridges. This research showed that the vulnerability of irregular RC bridges is significantly sensitive to the incidence angle of the earthquake. Mosleh et al. [28] employed a probabilistic approach to developing seismic fragility curves for pre-1990 highway RC bridges in Iran. The obtained results showed that the structural characteristics significantly impacted the seismic vulnerability of the studied bridges [28]. Rasouli et al. [29] proposed a performance-based design method for continuous span bridges with unequal height isolated hollow RC piers. The outcome of this study showed that the characterisitcs of pier cross section and Lead Rubber Bearings (LRBs) are important factors to achieve a uniform ductility demand and performance level in all piers. State-of-the-art studies on the seismic behaviour of irregular RC bridges have been reviewed comprehensively in [30].

1.1 Shortcomings in Previous Studies

In most previous studies, the higher demand absorption of the stiffer bridge piers and their higher likelihood of failure is pronounced. Moreover, the design/strengthening approaches mentioned above are all concerned with mitigating the concentration of damage in shorter piers. However, different height arrangements of piers might alter the seismic response of bridge piers and amplify the unbalanced damage accumulation in piers of varying heights. As a result, depending on varied circumstances of adjacent piers, the failure sequence of piers might be different, and critical piers (i.e., shorter piers) might become less or more vulnerable than other piers. Moreover, the unequal distribution of imposed masses along the length of the superstructure can induce unbalanced inertia

forces on piers of unequal heights. This can add to the complexity associated with the seismic response analysis of irregular concrete bridges. Nevertheless, only a few studies have been dedicated to studying the nonlinear dynamic response of various irregular multi-span bridge typologies, particularly those with different height arrangements of piers. This shows that the existing literature in this area is still inadequate, and therefore, there is a necessity for further investigation on seismic performance of multi-span irregular bridges with varied layouts. One of the main reasons for such shortcomings in previous studies was the limitations in the available numerical models, which have been addressed in this paper and discussed in the next section.

1.2 Research Contribution and Novelty

One of the crucial steps toward evaluating the nonlinear dynamic response and seismic vulnerability of irregular RC bridges is the development of advanced numerical models, which are reliable and realistic. To address the shortcomings (mentioned above) in the literature, an advanced 3D nonlinear finite element modelling technique is developed in OpenSees [31] to simulate the nonlinear dynamic response of irregular multi-span RC bridges. This numerical model is capable of accounting for the inelastic buckling and low-cycle high amplitude fatigue of longitudinal bars, which is able to capture multiple failure modes in bridge components. Using this model and by altering the arrangement of short, medium and tall bents, the influence of the height pattern of piers on nonlinear dynamic response, sequential failure, and vulnerability of multi-span RC bridges is investigated. Moreover, assuming a target axial force ratio of piers, the influence of equal and unequal distribution of super-imposed masses on seismic performance and failure sequence of irregular multi-span RC bridges is investigated and compared with the influence of stiffness irregularity.

The following section (Section 2) of the paper presents the details of the benchmark bridge specimen, proposed three-dimensional fibre-based finite element modelling technique and verification results. The remainder of the paper is arranged as follows: in Section 3, details of the selected irregular bridge layouts are described. Following that, Section 4 presents the nonlinear pushover analysis results of different bents, and Section 5 provides elastic modal analysis results in terms of modal periods and modal mass participation. Subsequently, in Section 6, incremental dynamic analyses (IDAs) results are presented and discussed. Finally, in Section 7, the failure probability of the selected bridge layouts is analysed and compared. The paper concludes by highlighting the main findings and remarks.

2. Bridge Prototype and Finite Element Modelling

2.1 Details of the Prototype RC Bridge Specimen

Fig. 1 shows the geometry and details of the prototype RC bridge system considered in this study as a benchmark for investigating the nonlinear dynamic behaviour and failure mechanisms of multi-span irregular RC bridges. This bridge system was tested on shake table facility at the University of Nevada, Reno [32]. To conduct the shake table tests, each bridge bent was placed on a separate shake table, and the seismic response of the whole bridge system was tested in the transverse direction. Further details about the experimental setup of this experiment are available in [32].

As Fig. 1 (a) shows, the two-span prototype bridge is supported on three double-column bents of varying heights. This prototype bridge system represents a two-span middle frame of a multi-span RC bridge [32]. The span length is 914.0 cm; the total bridge length is 2050.0 cm; the clear height of the piers from the top of the foundation is 182.9 cm, 243.8 cm and 152.4 cm for bent 1, bent 2

and bent 3, respectively. These heights translate to the aspect ratio of 2.5 to 4 from the shortest columns to the tallest. The depth and length of cap beams were 38 cm and 249 cm, respectively. In each span, the superstructure is composed of three deck beams with a width of 76.2 cm and a depth of 35.6 cm. Six 9.1 tons, two 2.3 tons, and two 10.8 tons concrete blocks are placed on the superstructure as super-imposed weights. These superimposed weights and the self-weight of the structure were used in the experiment to induce an approximately 8.2% axial force ratio on each bridge column.

Fig. 2 shows the details of each bent and reinforcement layout of piers. The cross-sectional details of all columns are the same, where the diameter is 30.5 cm; longitudinal reinforcements are sixteen 0.95 cm rebars; the spiral reinforcements are 0.95 cm (W 2.9) bars with a spiral pitch of 3.2 cm, and a clear cover thickness of 1.9 cm. This reinforcement layout provides approximately 1.56% longitudinal reinforcement ratio and 0.9% spiral reinforcement ratio in each column. All reinforcements used in the bridge were Grade 60 steel rebars. The average compressive strength of cylindrical concrete samples at the end of shake table tests was 40.8, 49.8 and 33 MPa for columns, beams, and footings, respectively. Further details are shown in Fig. 2.

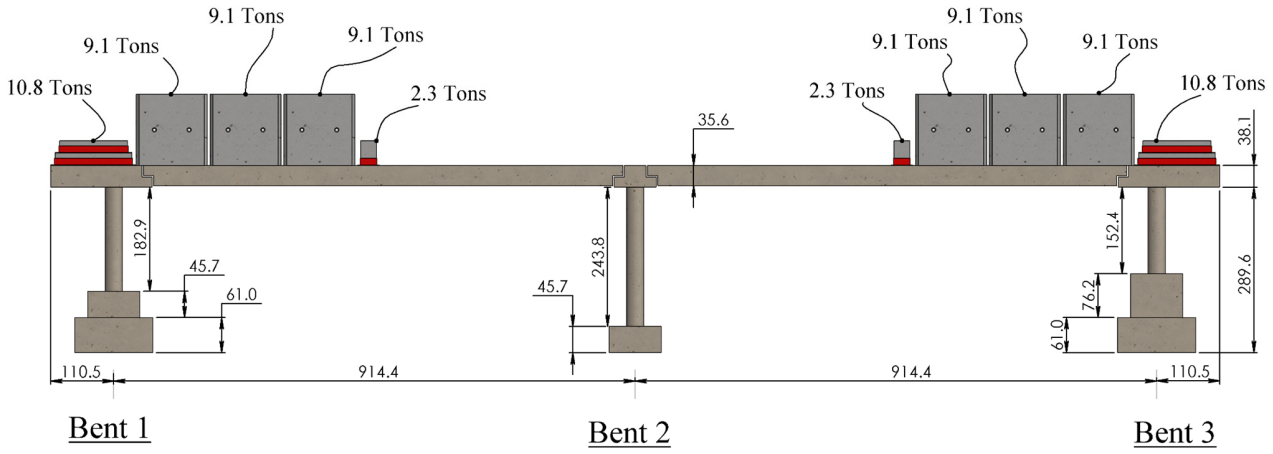

(a)

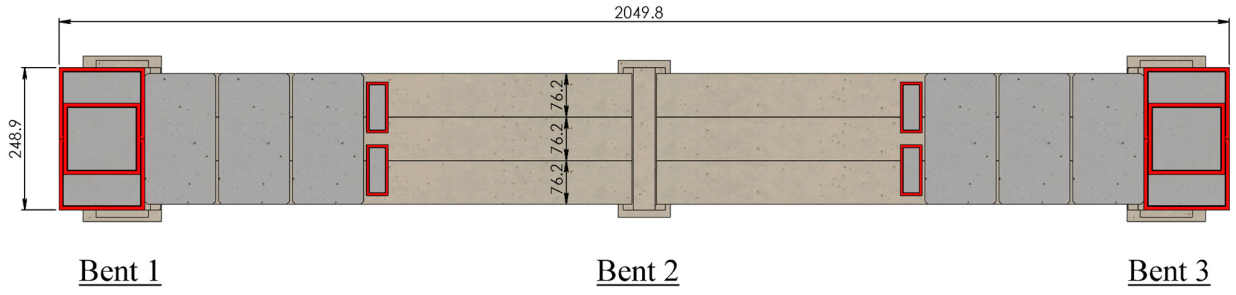

(b)

Fig. 1. Geometry and configuration of two-span RC bridge tested in University of Nevada: (a) longitudinal view, and (b) plan view (dimensions in cm)

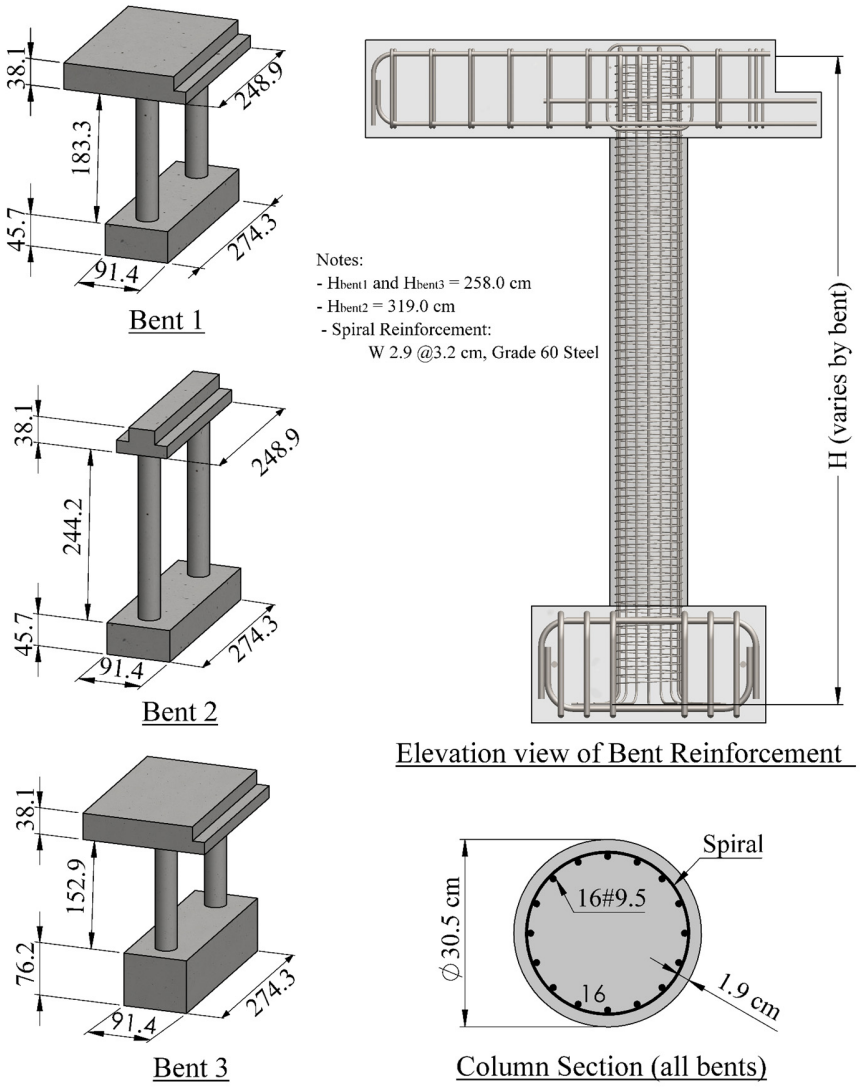

Fig. 2. Structural details of bents and columns (dimensions in cm)

2.2 Finite Element Modelling and Verification

To model seismic performance and failure mechanism of unequal pier height multi-span RC bridges, a 3D nonlinear finite element model of the benchmark RC bridge is developed using the OpenSees. Fig. 3 shows the nodal configuration of the developed Finite Element (FE) model of the bridge system. As Fig. 3 shows, each element is modelled using a series of nonlinear beam-column elements in its centreline. The deck and cap beams are modelled by elastic beam-column elements as they remained in the elastic range during the shake table tests [32]. To apply the superimposed masses in their corresponding mass centres, extra nodes are defined (nodes 441, 461, 471, 481, 491, 591, 601, 611, 621, and 641) and connected to their corresponding nodes in deck elements through rigid links. This way, the superimposed masses will be applied at a distance from the deck, which consequently increases the accuracy of simulations by inducing realistic dynamic forces on the bridge superstructure. The self-weight mass of each member is lumped at the structural nodes. All the connections, including the deck beam to cap beam connections, cap beam to column connections, and column to footing connections, are considered to be fully fixed. It should be noted that the soil-structure interaction is not considered in this study.

The force-based nonlinear beam-column element developed by Kashani et al. [33] is implemented in the model to simulate the nonlinear structural behaviour of piers. This model can accurately simulate the inelastic buckling behaviour and low-cycle fatigue degradation of vertical reinforcements. The accuracy of this model in simulating the cyclic response of bridge piers is verified by an extensive set of experimental results. Moreover, this model has been used successfully to investigate the vulnerability of rectangular and circular bridge piers subject to sequential seismic events [34-35]. Further details are available in [33].

As an example, the details of the beam-column element used for the columns of the intermediate bent (bent 2) are shown in Fig .4. As shown in Fig. 4, each pier consists of six elements: two zero-length section elements, two force-based elements at top and bottom, a force-based element in the middle, and a rigid link at the top. The zero-length section elements are employed to simulate the strain penetration effects and bar slippage at the bottom and top anchorage zones [36]. The bottom and top force-based elements with three Integration Points (IPs) are used to address the localisation problem due to the softening behaviour of reinforcing bars in compression [33]. The length of each top and bottom force-based element is considered six times the effective buckling length (L_{eff}) of longitudinal reinforcing bars, where L_{eff} is calculated based on the procedure presented in [37]. The detailed information about this method is available in [33]. The middle element is a force-based element with five IPs [38]. The topmost element of each column is a rigid link to consider the rigid connection zone between the column and cap beam.

The nonlinear behaviour of bridge piers is defined through the fibre sections in each IPs, where the cross-section of the column is decomposed into several fibres (patches), including unconfined concrete fibres, confined concrete fibres and reinforcing bar fibres. The uniaxial material *Concrete 04*, available in the OpenSees is used for the unconfined and confined concrete. The confinement effects on strength and ductility of concrete are considered employing Mander et al. model [39]. The nonlinear stress-strain behaviour of reinforcing bars is modelled using the buckling model proposed by Kashani et al. [40]. This model can simulate the inelastic buckling and low-cycle fatigue degradation of reinforcing bars. Further details are available in [40].

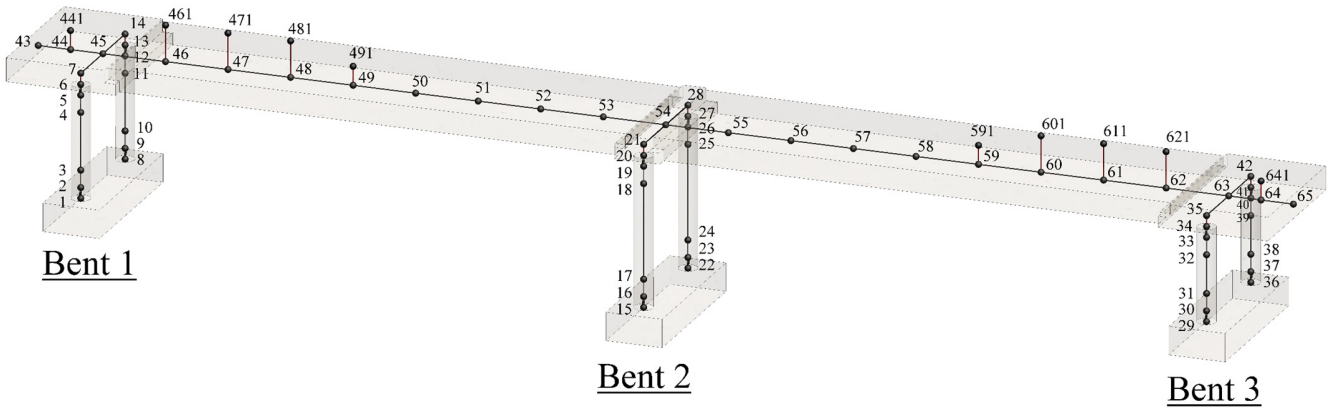

Fig. 3. Nodal configuration of 3D nonlinear finite element model

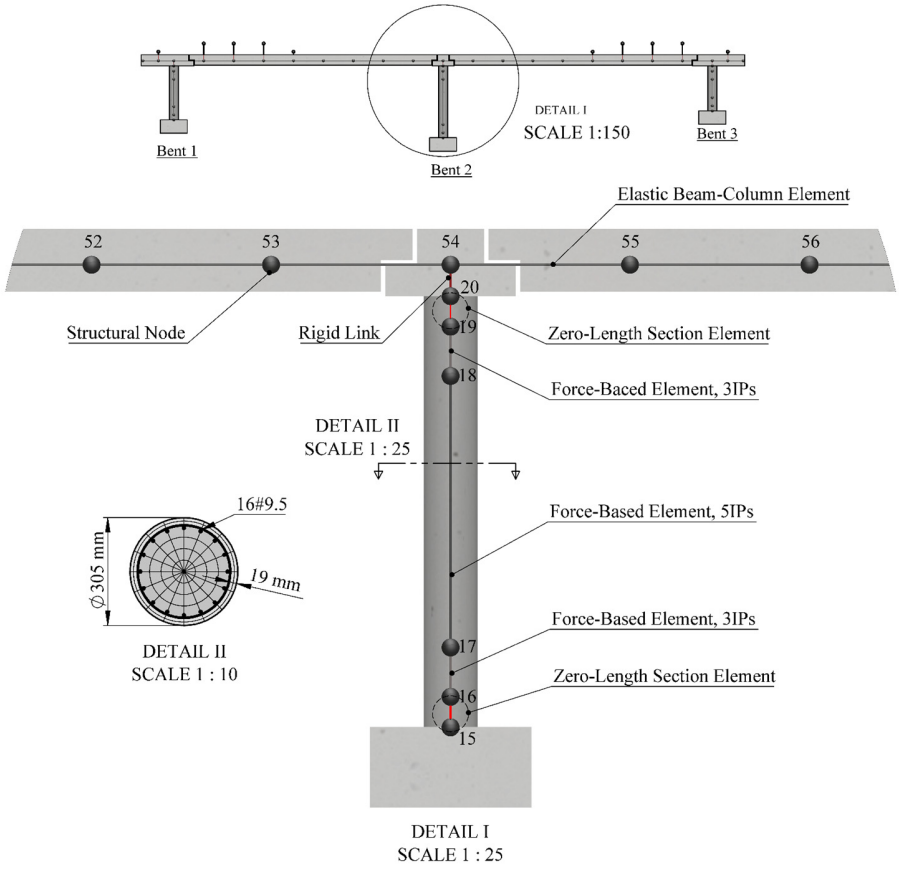

Fig. 4. Details of the nonlinear beam-column model of piers and deck

Johnson et al. [32] conducted two different sets of shake table tests, including low amplitude tests and high amplitude tests. The first set was a series of 11 (test No. 1 to test No. 11) sequential shake table tests. The intensity of test motions for the low amplitude tests was adjusted such that the maximum achieved moment in the columns remained below half of the effective yield moment of the columns to ensure that the system would experience no damage before the high amplitude tests. The bridge was then subjected to high-amplitude tests to observe the system response up to its failure. These later tests were composed of nine records of increasing amplitude (tests 12 to 20), where each record duration and time steps were 25 seconds and 0.01 seconds, respectively. Further details are available in [32].

The high-amplitude tests chose to verify the developed three-dimensional nonlinear finite element model. Following the recommendation given in [32], the displacement history achieved on three shake tables is used to validate the numerical model in this study. This is because the interaction between the bridge system and shake tables leads to incoherent recorded acceleration response on these three shake tables. Therefore, to conduct multiple support excitation and satisfy the equations of motions, the achieved displacement history from the measured acceleration history of tables is used as input in OpenSees to simulate the superstructure response. The input displacement history of the three shake tables for nine high-amplitude tests is shown in Fig .5.

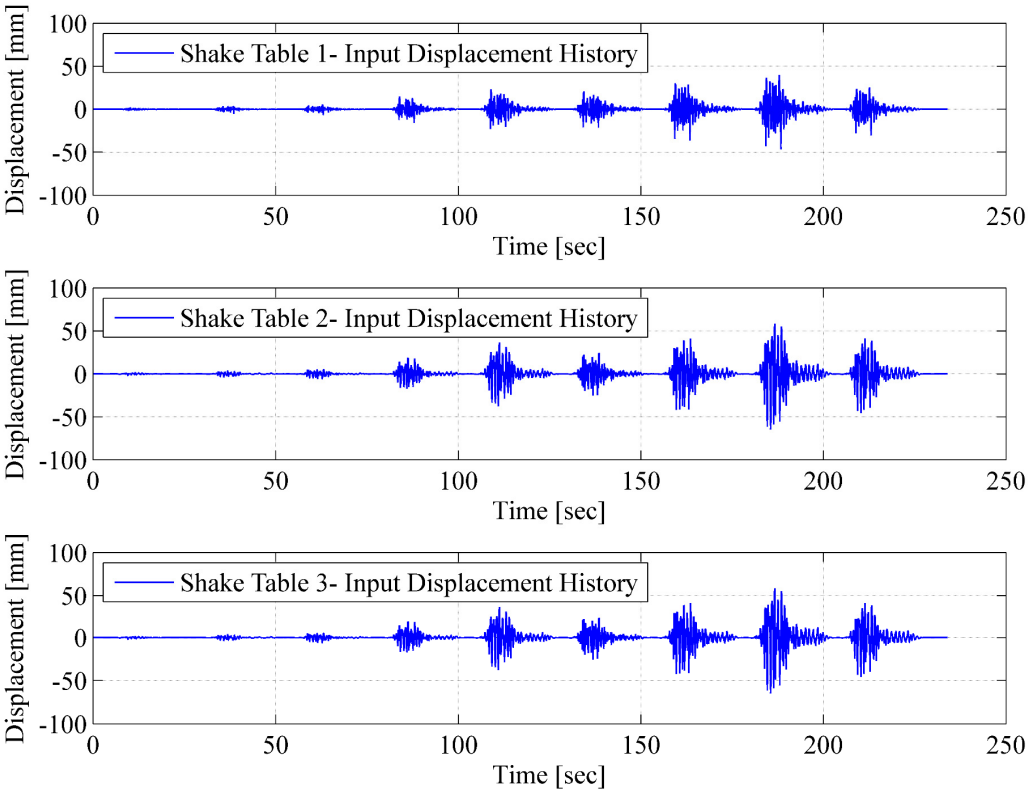

Fig. 5. Input displacement history for validation of the proposed 3D finite element model

Fig. 6 compares the simulated top (superstructure) acceleration response of each bent with the corresponding response measured in the experiment during test 17. As shown in Fig .6, the simulated response of each bent compares well with the corresponding measured response. This confirms that the developed 3D finite element model can accurately track the nonlinear response of the case-study bridge system. In the next section, this model is used to carry out nonlinear pushover and dynamic analyses on irregular bridges with different layouts of piers.

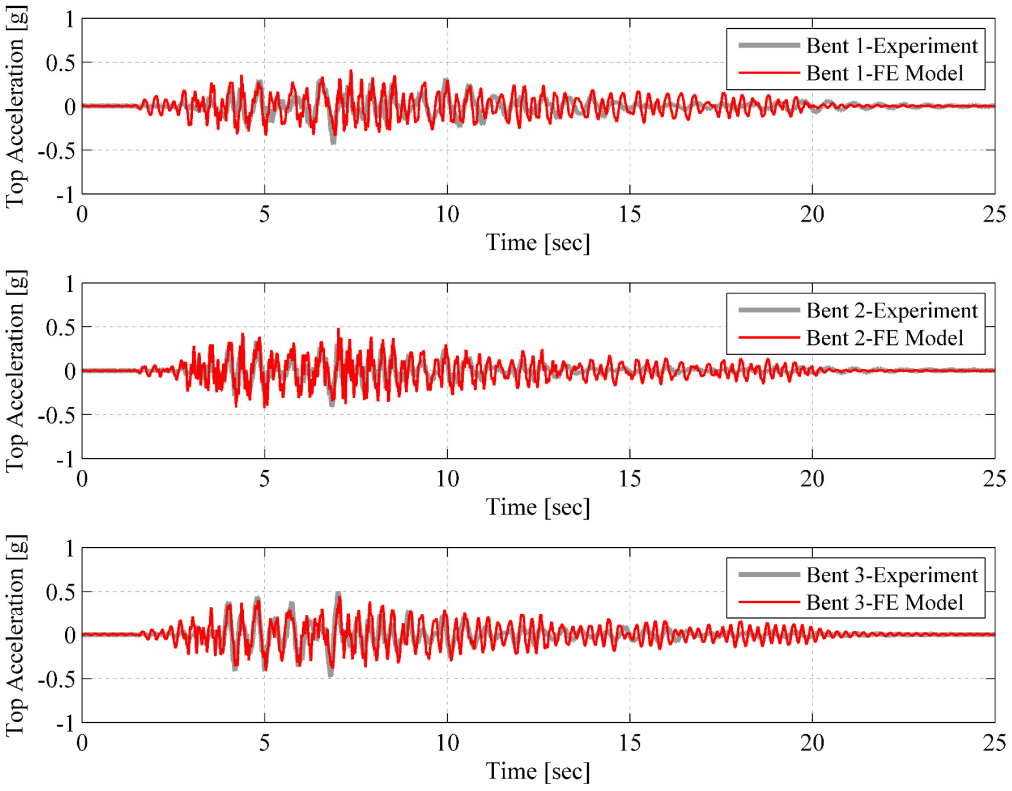

Fig. 6. Validation results for acceleration response of superstructure during test 17

3. Selected Irregular Bridge Layouts

Depending on the topographical conditions, various pier height, and their arrangements in adjacent bents of a frame might be implemented to adapt to the terrain variation. However, varied arrangements of pier height in adjacent bents within a bridge frame might change the pattern of absorbed unbalanced ductility demands in different bents. This might change the sequence of failure of bridge piers with varying heights in a multi-span RC bridge, leading to distinctive bridge failure mechanisms.

In order to investigate the influence of the layout of multi-span RC bridges with height irregularity, three different bridge configurations labelled as A1, B1 and C1 are selected, as shown in Fig. 7.

The numerical model of these bridges is established using the validated three-dimensional finite element model. The dimensions of these bridges are assumed to be similar to the benchmark bridge, and only the arrangement of piers is altered. Bridge A1 is the same bridge as the benchmark bridge where the tallest piers are in the middle (at bent 2), and the medium-height and the shorter piers are located on the left and right side of the bridge, respectively (i.e., at bent 1 and bent 3). In bridge B1, which has the same details and dimensions as bridge A1, the taller piers are located in bent 1; the medium-height piers are located in bent 2, and the shorter piers are at bent 3. Finally, in bridge C1, the shortest piers are placed at the middle of the bridge, the tallest piers are placed at bent 1, and the others are at bent 3.

A regular bridge (labelled as A0) is also considered as a reference layout for bridges A1, B1 and C1. The height of all the piers of this bridge is assumed to be equal to that of columns in the middle bent of the benchmark bridge. The other conditions, such as the distribution of super-imposed masses and geometrical details, are kept the same as the benchmark bridge. The nonlinear dynamic and seismic fragility analysis results of this regular bridge are compared with those of bridges A1 , B1 and C1 in Sections 6 and 7, respectively.

Other than A1, B1 and C1 layouts, three additional layouts (A2, B2 and C2) are also considered to investigate the influence of unbalanced inertial forces acting on different bents due to the varied tributary mass on each bent. The details and configuration of these bridge layouts are similar to A1, B1 and C1 layouts, but the super-imposed masses are assumed to be equally distributed among the bents. To this end, the summation of all the super-imposed weights shown in Fig. 1(a) was divided by six to have all the piers with equal tributary mass values. It is noteworthy that the main goal behind considering these three cases is to compare their analysis outputs with those of their

corresponding layouts with unequal mass distribution status (i.e., bridges a1, B1 and C1). Therefore, no reference regular bridge for these cases is considered in this study.

The summary of the case-study bridge layouts is listed in Table 1.

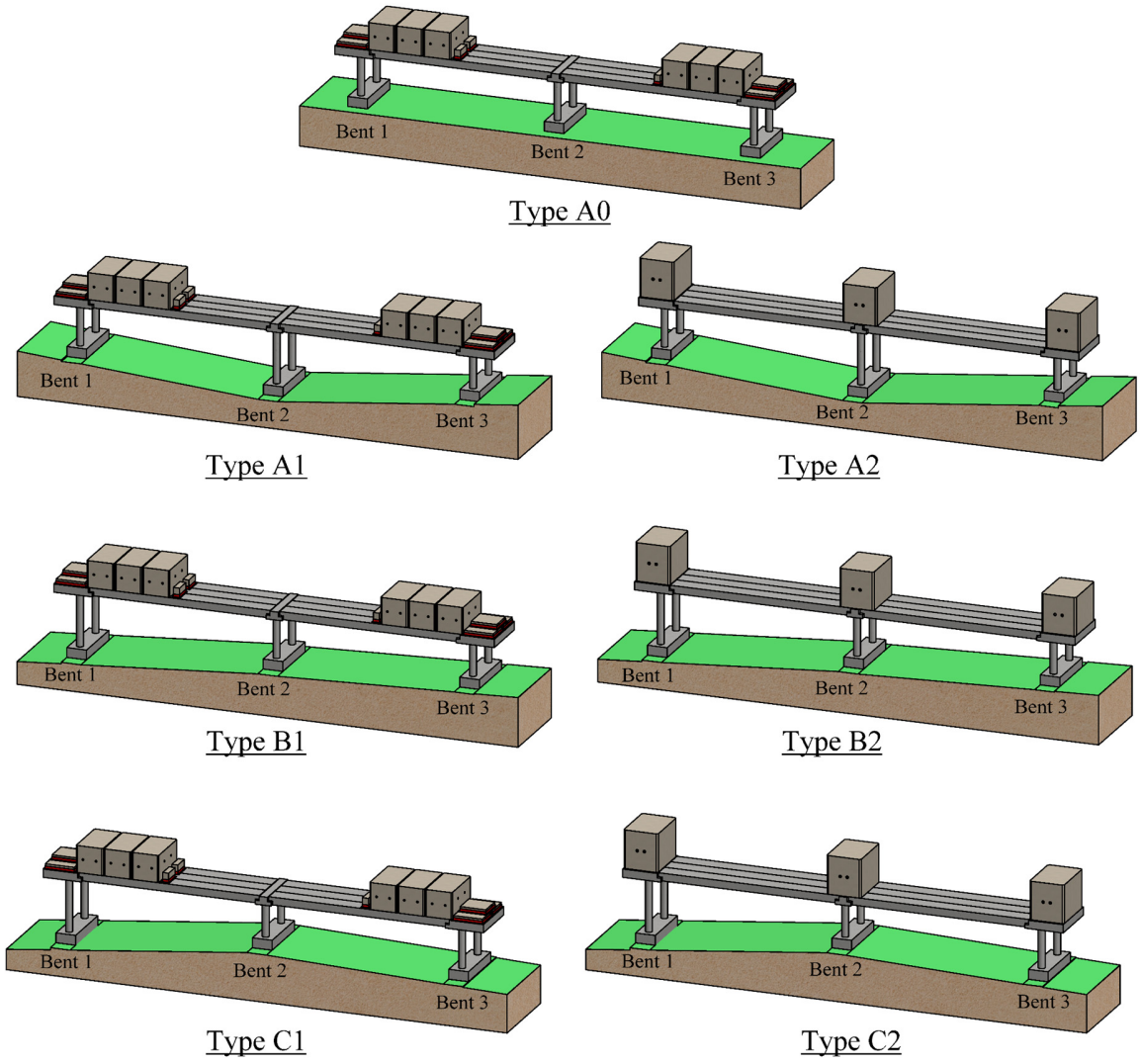

Fig. 7. Case-study RC bridges with varied substructure stiffness configurations

Table 1. Summarised characteristics of selected bridge layouts

Bridge Layout	Mass Distribution Status	Stiffness Regularity Status	Pier Height Status		
			Bent 1	Bent 2	Bent 3
A0	unequal	regular	medium	medium	medium
A1	unequal	irregular	medium	tall	short
A2	equal	irregular	medium	tall	short
B1	unequal	irregular	tall	medium	short
B2	equal	irregular	tall	medium	short
C1	unequal	irregular	tall	short	medium
C2	equal	irregular	Tall	short	medium

4. Nonlinear Pushover Analysis, Results and Discussion

The damage limit states of piers in each bent are determined using the nonlinear pushover analysis. This study considers five damage limit states such as, rebar yielding, concrete spalling, core concrete crushing, rebar fracture, and 20% strength loss. These damage limit states have been successfully correlated with drift ratio thresholds corresponding to slight, moderate, extensive and complete collapse damage states, and used in seismic vulnerability analysis of uncorroded and corroded RC structures [41-42].

The rebar yielding limit state reaches when the outmost tensile reinforcement at the critical section of the bridge pier yields. The concrete spalling occurs when the outmost compression fibre of cover concrete reaches the spalling strain. Here, this strain limit is assumed as 0.004 [43]. Rebar fracture takes place when the tensile strain of longitudinal reinforcement reaches 0.16, according

to [32]. Finally, the core concrete crushing corresponds to the fracture of the first confining steel where the compressive strain of extreme core concrete fibres reaches ε_{cu} according to Eq. (1) [43]:

$$\varepsilon_{cu} = 0.004 + 1.4\left[\frac{\rho_s f_{y,s}\,\varepsilon_{u,s}}{f_{c,c}}\right] \quad (1).$$

In Eq. (1), ρ_s, $f_{y,s}$ and $\varepsilon_{u,s}$ are volumetric ratio, yield strength, and tensile strain at peak stress of spiral reinforcements, respectively, and $f_{c,c}$ is the compressive strength of confined concrete.

To perform pushover analysis, the finite element model of each bent of the benchmark bridge is extracted from the 3D model of the bridge and subjected to displacement-control loading at the level of column tip. The P-Delt effect is considered in the analyses. Moreover, column to foundation connections and the column to caping beam connections are considered to be fully fixed. Fig. 8 shows the capacity curves of each bent in bridges A1 and A2, bridges B1 and B2, and bridges C1 and C2 from the pushover analysis results. The statistics shown in Fig. 8 are summarised in Table 2. It should be highlighted that, as the structural details and axial force ratio of columns in A1, B1 and C1 bridges are the same as their corresponding cases (A2, B2 and C2), their capacity curves are equivalent. In addition to the four considered damage limit states, the onset of a 20% drop in peak lateral force is also shown on the capacity curve of each bent. As the results show, the fracture of rebars does not occur in any of the bents, and core concrete crushing governs the failure of all the bents.

Fig. 8(a) indicates that the associated drift with the crushing of core concrete in piers of bent 3 is lower than those of bent 1 and bent 2. This is because the piers of bent 3 are the shortest of columns, with the minor aspect ratio among the other bents. The lesser ductility of shorter columns exposes them to higher ductility demands and a possibly earlier collapse than other bents. However, as discussed in Section 6, the layout of irregular bridges determines the critical columns of an

irregular multi-span RC bridge. Nevertheless, the associate drift with the onset of core concrete crushing shown in Fig. 8 for each bent will be used in Section 6 to evaluate the failure sequence of bents in the studied bridges.

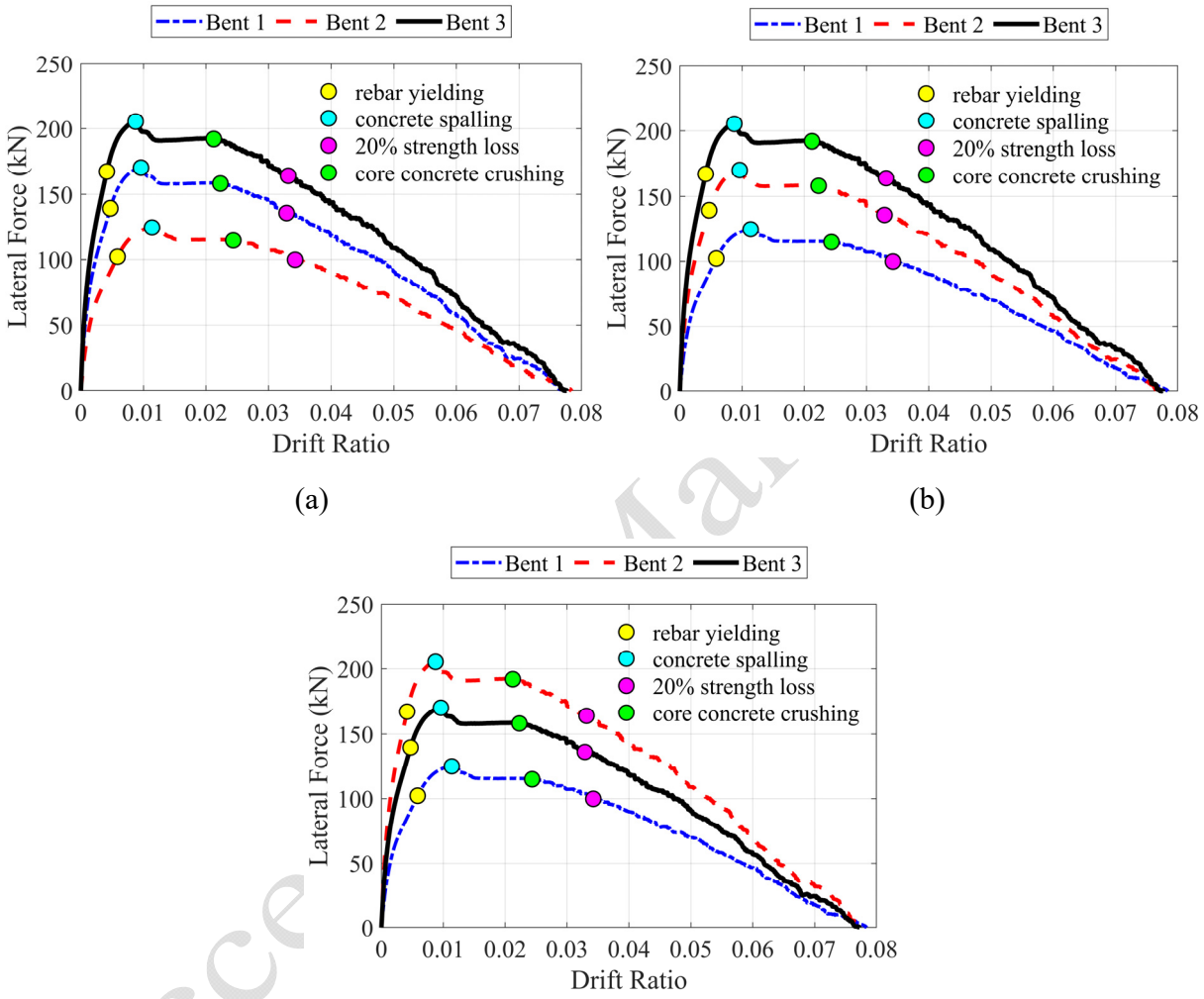

Fig. 8. Comparing the capacity curves of individual bents: (a) bridge A1 and A2; (b) bridge B1 and B2, and (c) bridge C1 and C2

Table 2. Associated drift ratios with considered damage limit states

Bridge Layout	Bent	Drift ratio at rebar yielding	Drift ratio at concrete spalling	Drift ratio at core concrete crushing	Drift ratio at 20% capacity loss
A1	Bent 1	0.005	0.010	0.022	0.033
	Bent 2	0.006	0.011	0.024	0.034
	Bent 3	0.004	0.009	0.021	0.033
B1	Bent 1	0.006	0.011	0.024	0.034
	Bent 2	0.005	0.010	0.022	0.033
	Bent 3	0.004	0.009	0.021	0.033
C1	Bent 1	0.006	0.011	0.024	0.034
	Bent 2	0.004	0.009	0.021	0.033
	Bent 3	0.005	0.010	0.022	0.033

5. Elastic Modal Analysis

In order to investigate the transverse seismic response of the selected RC bridge layouts, elastic modal analyses are performed to obtain their modal characteristics (including modal periods and mass participation). The elastic modal analyses are conducted using the uncracked state of the concrete. It is noteworthy that, because the focus of the current study is on the transverse seismic behaviour of the studied irregular RC bridges, only the modal characteristics in transverse vibration are discussed.

The elastic modal analysis results show that in bridge A1, mode 2 and mode 4 are two predominant transverse modes with a period of T_2=0.262 sec and T_4=0.193 sec, respectively. Moreover, the obtained results show that the two fundamental modes of vibration of bridge B1 in the transverse

direction are modes 1 and 4, with T_1=0.313 sec and T_4=0.185 sec. In this bridge, the second and third vibration modes are in the longitudinal direction and are not evaluated here. Same as bridge B1, the fundamental period of bridge C1 belongs to the transverse vibration. However, the second predominant transverse mode of this bridge is mode 3.

The modal mass participation of predominant transverse vibration modes is calculated and shown in Fig. 9. Moreover, the modal periods and quantified percentages of modal masses are tabulated in Table 3. Fig. 9 indicates that different short and tall bridge piers combinations result in significantly varied mass participation in different transverse modes. For instance, the medium-tall-short height arrangement of bridge piers (bridge A1) causes the significantly higher mass participation of the predominant transverse mode (i.e., mode 2) by approximately 78.8% (Table 3). Conversely, the tall-short-medium height arrangement of piers (bridge C1) leads to the greater mass participation of the second prevailing transverse mode (i.e., mode 4) by about 65.7%. However, the modal mass participation of the first and second predominant transverse modes of bridge B1 are near equal by approximately 55.5% and 44.4%, respectively.

Overall, the above discussion implies that different arrangements of piers of varying heights can significantly affect the dynamic behaviour of irregular multiple-frame RC bridges. Consequently, in a seismic event, the unbalanced lateral displacement demand of different bents of a multi-span irregular RC bridge will depend on the height arrangement of piers. Therefore, the typical presumption of a higher failure probability of shorter piers due to their higher seismic force absorption might be incorrect.

In the next section, the seismic performance of selected bridge layouts is investigated through nonlinear dynamic analyses, which will help effectively analyse the complex seismic response of irregular RC bridges.

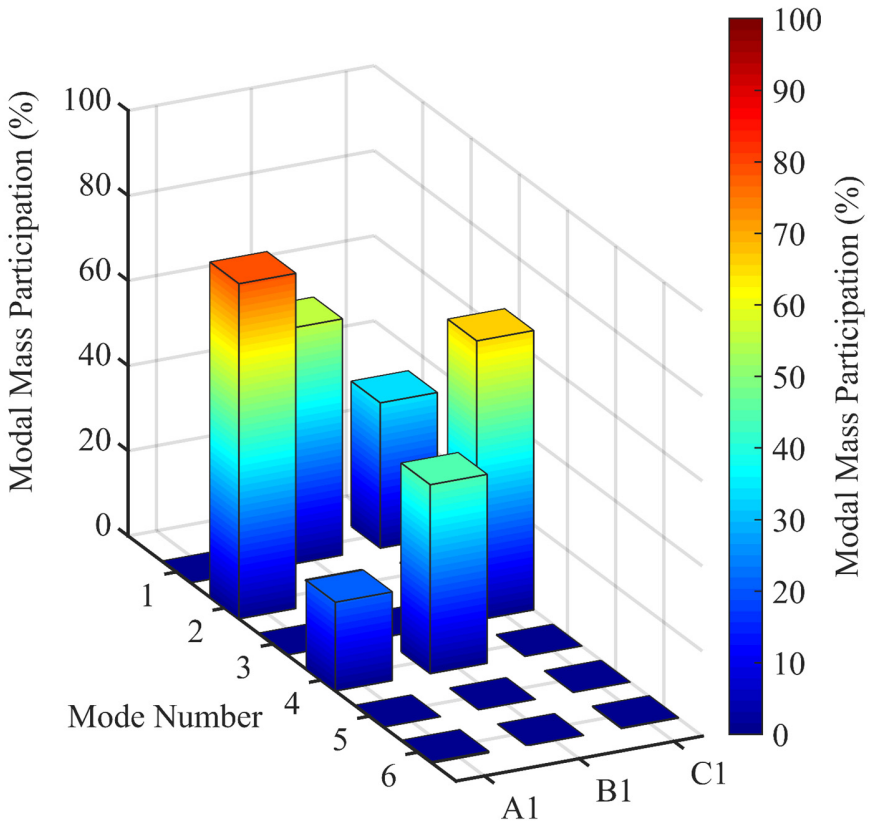

Fig. 9. Modal mass participation of predominant transverse modes in bridges types A1, B1, and C1

Table 3. Modal periods and mass participation

Mode	Bridge A1		Bridge B1		Bridge C1	
	T (Sec)	M (%)	T (Sec)	M (%)	T (Sec)	M (%)
1	0.304	-	0.313	55.5	0.296	34.15
2	0.262	78.8	0.275	-	0.264	-
3	0.202	-	0.205	-	0.219	65.7
4	0.193	20.9	0.185	44.4	0.209	-

6. Incremental Dynamic Analysis (IDA), Results, and Discussion

IDA is recognised as an efficient tool to evaluate the seismic performance of structures, as it enables monitoring the seismic response of a structure from the elastic range to the failure [44]. To perform the IDA, a sufficient number of ground motion records are scaled-up in terms of an intensity measure (IM); then, the maximum structural response associated with each input IM of an earthquake record is generally described as an engineering demand parameter (EDP). In the current study, the nonlinear dynamic behaviour of studied bridge specimens is investigated using the IDA, where the peak ground acceleration (PGA) is considered the IM and the maximum drift ratio of bridge bents is adopted as the EDP. The maximum drift ratio of each bent is calculated as the maximum tip displacement of the bent piers divided by the height of the same piers. For the dynamic analyses, the mass and stiffness proportional damping method (the Rayleigh damping method) is used with the critical damping of 4.3% [41] for the first and third transverse vibration modes.

In the following sub-sections, the characteristics of the selected ground motions and the outcome of IDAs are discussed.

6.1 Ground Motion Selection

The first step in conducting IDA is to select a sufficient number of ground motion records to consider the uncertainties associated with earthquakes of varied frequency contents. In this study, 16 record pairs (32 records in total) are selected from the far-field ground motion records provided in FEMA P695 [45]. Table 4 provides the characteristics of the selected ground motions records. Moreover, in Fig. 10, the spectral acceleration response of the selected ground motions is shown.

To conduct IDAs, the selected records with increasing IM levels (from 0 to 1g) are applied to the case-study bridges. In the next section, the results of IDAs are presented and discussed.

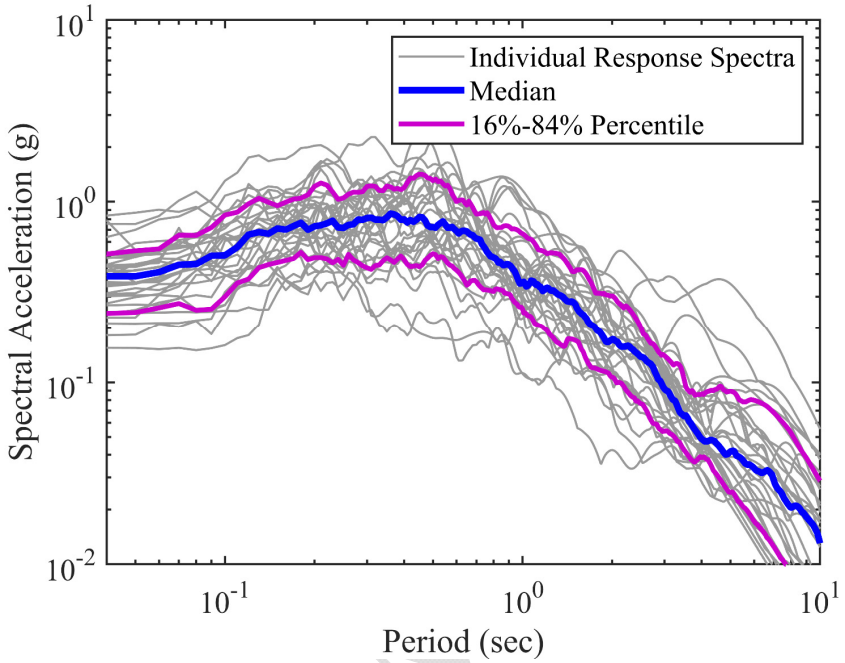

Fig. 10. Spectral acceleration response of the selected ground motion suite

6.2 Analysis Results of Bridges A1, B1, and C1

6.2.1 IDA Results at the System Level

Figs. (11-13) present the IDA results of A1, B1 and C1 bridge layouts. In each figure, the IDA response of each bent and the comparative summarised responses of three bents of the same bridge are provided. Moreover, the median IDA response of bridge A0 (regular bridge) is presented in Figs. 11(d), 12(d) and 13(d) and compared with that of considered irregular bridges.

Figs. 11(a-c) show the IDA curves of bent 1, bent 2, and bent 3 of bridge A1, respectively. In each figure, individual IDA curves, as well as the summarised IDA responses, are plotted. Furthermore,

the collapse threshold drift ratio is shown by a vertical solid line. As discussed in section 4, this threshold is defined here as the associated drift with the failure of core concrete. Fig. 11(a) shows that the range of individual PGAs associated with the collapse threshold of bent 1 varies from approximately 0.2g to 0.7g. This range is from about 0.35g to 0.75g for bent 2 (Fig. 11(b)) and from approximately 0.3g to 0.68g for bent 3 (Fig. 11(c)). In Fig. 11(d), the median IDA responses of all bents (extracted from Figs. 11(a-c)) of bridge A1 are compared. Furthermore, the median failure point of each bent is also shown in the corresponding median IDA curves. The median failure point is obtained from the intersection of collapse threshold and the median IDA response of each bent, shown in Figs. 11(a-c).

Table 4. Details of the selected ground motion records

No	NGA Event name/Event ID	Station ID	Magnitude	PGA_{max} (g)	PGV_{max} (cm/s)
1	Northridge	Beverly Hills - Mulhol	6.7	0.52	63
2	Northridge	Canyon Country-WLC	6.7	0.48	45
3	Duzce, Turkey	Bolu	7.1	0.82	62
4	Hector Mine	Hector	7.1	0.34	42
5	Imperial Valley	Delta	6.5	0.35	33
6	Kobe, Japan	Nishi-Akashi	6.9	0.51	37
7	Kobe, Japan	Shin-Osaka	6.9	0.24	38
8	Kocaeli, Turkey	Duzce	7.5	0.36	59
9	Kocaeli, Turkey	Arcelik	7.5	0.22	40
10	Landers	Yermo Fire Station	7.3	0.24	52
11	Landers	Coolwater	7.3	0.42	42
12	Loma Prieta	Gilroy Array #3	6.9	0.56	45
13	Superstition Hills	El Centro Imp. Co.	6.5	0.36	46
14	Superstition Hills	Poe Road (temp)	6.5	0.45	36
15	Chi-Chi, Taiwan	CHY101	7.6	0.44	115
16	Chi-Chi, Taiwan	TCU045	7.6	0.51	39

Fig. 11(d) shows that up to around PGA=0.55g, for a given IM level of input ground motions, bent 1 experiences higher drift ratios than other bents. This leads to the earlier failure of columns of bent 1, which corresponds approximately to PGA=0.37g. Moreover, Fig. 11(d) shows that the subsequent failure occurs in columns of bent 3, corresponding to about 0.46g in terms of the median input IMs. Finally, the following failure sequence will occur in columns of bent 2 at around PGA=0.52g. Therefore, it can be inferred from the results given in Fig. 11 that the failure sequence of columns of bridge A1 under the selected ground motions will be as: (*i*) medium height columns (bent 1); (*ii*) shortest of columns (bent 3), and (*iii*) tallest of columns (bent 2). This conclusion is consistent with the results of the elastic modal analysis presented in Section 5.

In Fig. 11(d), the median IDA results of bridge A0 (regular bridge) are also presented as a baseline. As all the bents are of equal height in this bridge, their IDA response is the same. Therefore, here a single median IDA curve representing the median IDA response of the intermediate bent of this bridge is presented and discussed. A simple comparison between the median IDA curve of bridge A0 and that of different bents of bridge A1 shown in Fig. 11(d) indicates that the associate PGA with the onset of plateau response of regular bridge is higher than that of the corresponding irregular bridge. Specifically, bent 1 in bridge A1, which has columns of the same height as bridge A0, experiences significantly higher drift rations for a given PGA. For instance, while the regular bridge reaches approximately 2.8% lateral drift under PGA= 0.5g, bent 1 of bridge A1 tolerates 4% drift for the same PGA level. This confirms the higher vulnerability of irregular bridges compared to the corresponding regular bridge.

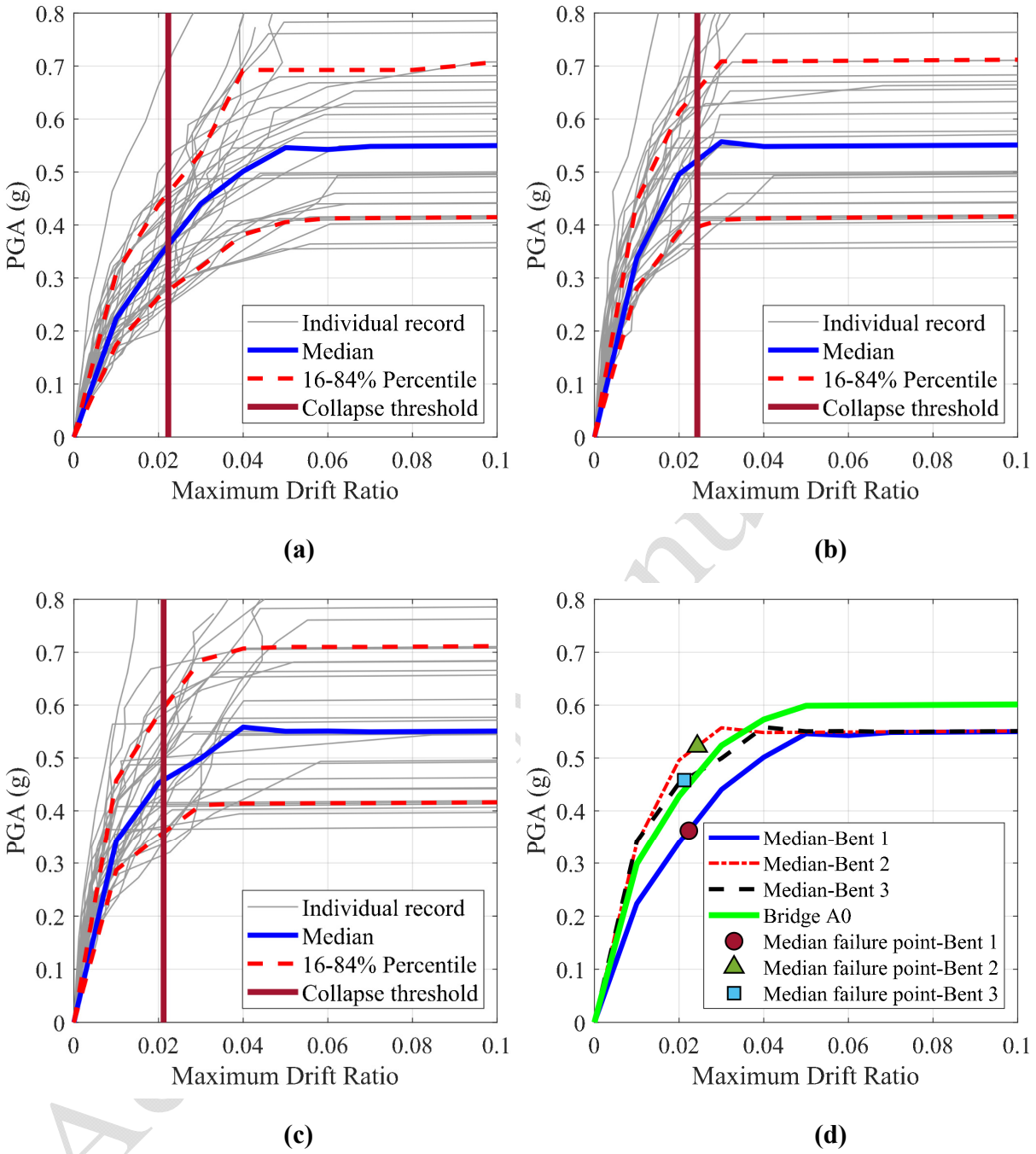

Fig. 11. IDA results of bridge A1: (a) response of medium-height bent (bent 1); (b) response of tall bent (bent 2); (c) response of short bent (bent 3), and (d) median response of all bents

Fig. 12 shows an exemplary hysteretic response of bents of bridge A1. A representative record of the median response of the critical bent (bent 1), the Northridge record, with PGA=0.35g, which

approximately corresponds to the median failure IM of this bent, is selected. As Fig. 12 shows, bent 1 tolerates the most significant ductility demand compared to the other bents, where under the selected record and IM level, bent 1 experiences more than 0.03 drift ratio while others sustain less than 0.015 drift ratio. This indicates the higher seismic vulnerability of bent 1, and confirms the results provided in Fig. 11(d).

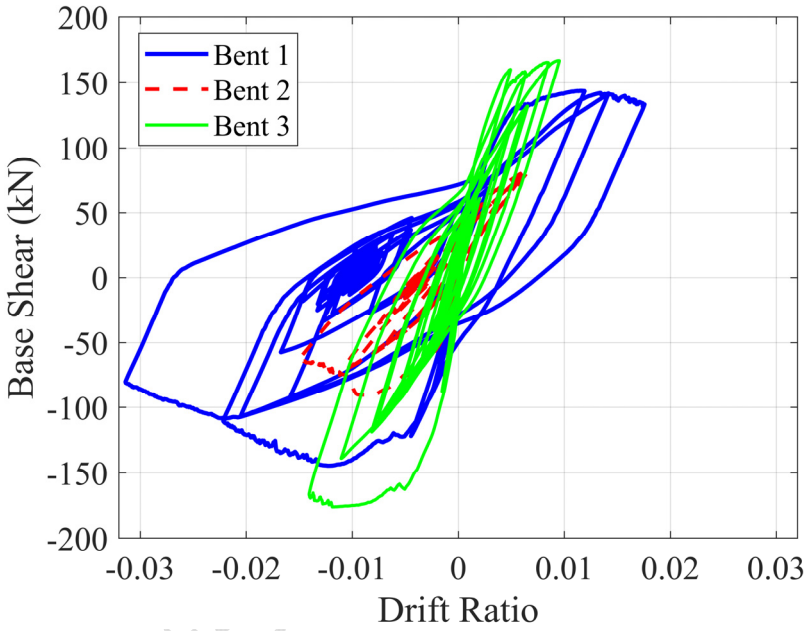

Fig. 12. An exemplary hysteretic response of individual bents of bridge A1 under Northridge ground motion

In Fig. 13, the IDA results of B1 bridge specimen are shown. A comparison between the median IDA curves of bent 1, bent 2 and bent 3 shows that in this bridge layout, taller columns placed in bent 1 reach their collapse threshold at approximately PGA=0.4g, which is lower than those of bent 2 and bent 3. However, the median failure PGAs of bent 2 and bent 3 are roughly the same, with a slightly lesser value for bent 2. This implies that, in bridge B2, the tallest columns will fail earlier than others, and subsequently, the medium height columns will be collapsed just before the short columns.

As shown in Fig. 13(d), prior to the beginning of plateau response, the median IDA response of bridge A0 approximately coincides with that of the medium-height bent of bridge B1, i.e., bent 2. However, as discussed above, as the collapse of bridge B2 is governed by the failure of the taller bent (bent 1), the plateau response of bent 2 starts at less drift ratio compared to that of its corresponding bents in bridge A0.

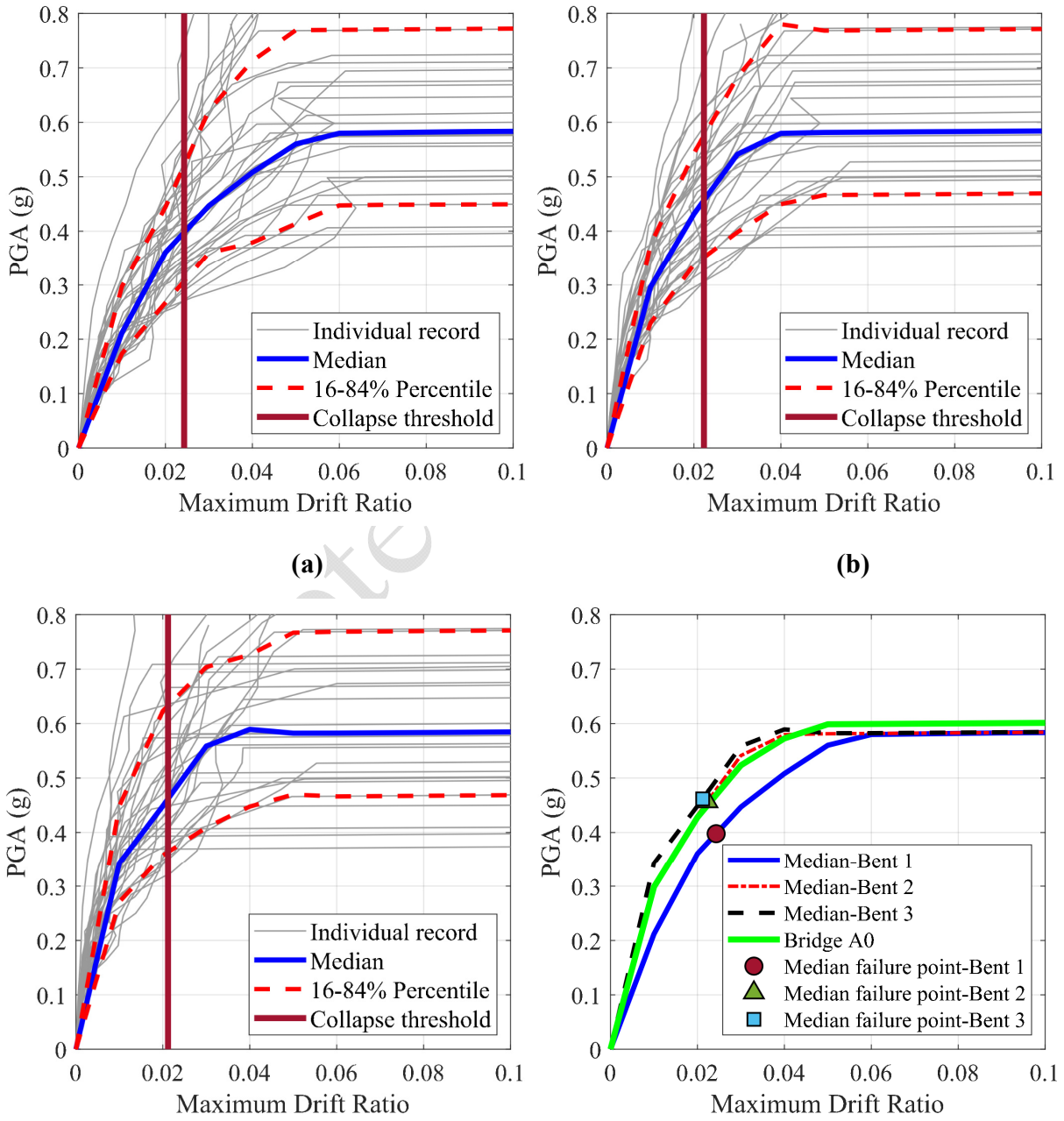

(c) **(d)**

Fig. 13. IDA results of bridge B1: (a) response of tall bent (bent 1); (b) response of medium-height bent (bent 2); (c) response of short bent (bent 3), and (d) median response of all bents

Fig. 14 shows the hysteretic response of individual bents of bridge B1 subject to Hector Mine ground motion under the median IM corresponding to the failure of bent 1, i.e. PGA=0.39g. This record was selected because the median IDA response of bent 1under this record is approximately the same as its median response shown in Fig. 13(d). As Fig. 14 shows, the taller columns placed in bent 1 of bridge B1 attract higher displacement demand and are prone to seismic failure prior to bent 2 and bent 3.Moreover, medium-height columns placed in bent 3 absorb greater inertia forces than shorter piers in this bridge. However, the distribution of seismic inertia demand between varied height bents depends significantly on the frequency content of input earthquake, and the results presented in this figure can not be generalised to other considered ground motions.

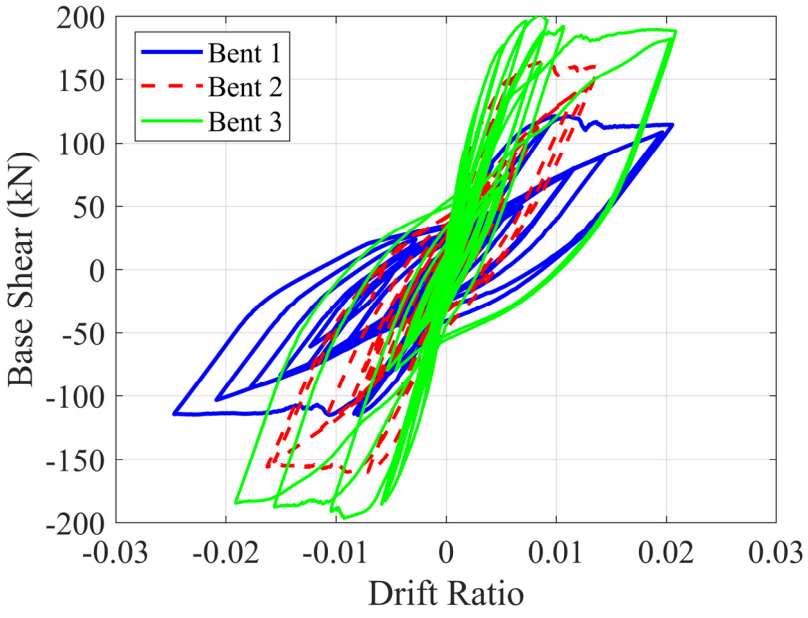

Fig. 14. An exemplary hysteretic response of individual bents of bridge B1 under Hector Mine ground motion

Fig. 15 presents the IDA results of bridge C1. Figs. 15(a-c) show the PGA-maximum drift ratio response of bent 1, bent 2, and bent 3 separately. Similar to those seen in Figs. 11 and 13, these figures show a wide range of PGAs associated with the collapse of each bent. This is due to the randomness associated with the frequency content of the selected ground motions. Despite the results obtained for A1 and B1 bridges (shown in Fig. 11(d) and Fig. 13(d)), Fig. 15(d) shows that for this case, the shorter columns (placed in bent 2) are critical and govern the failure of the bridge.

Moreover, based on the results, the tallest columns (placed in bent 1) will fail subsequently at approximately PGA=0.45g, and finally, the columns in bent 3 will fail at around PGA=0.49g. Therefore, the predicted failure sequence in columns of bridge C1 will be as (*i*) shortest of columns; (*ii*) tallest of columns; and (*iii*) medium-height columns.

Furthermore, Fig. 15(d) shows that the median IDA drift ratio of the regular bridge (bridge A0) is slightly lesser than the shortest bent of bridge C1 for a given PGA. Additionally, the onset of the plateaued response of medium-height bent 2 takes place in a less drift ratio than bridge A0. These results imply the higher vulnerability of irregular bridge C1 with the corresponding regular bridge.

The three above discussed cases demonstrate that the general assumption that the shortest piers in an irregular bridge fail in advance to other taller piers cannot always be the case, and depending on the complex geometry and ground motion characteristics, the sequence of failure in bridge piers can be different.

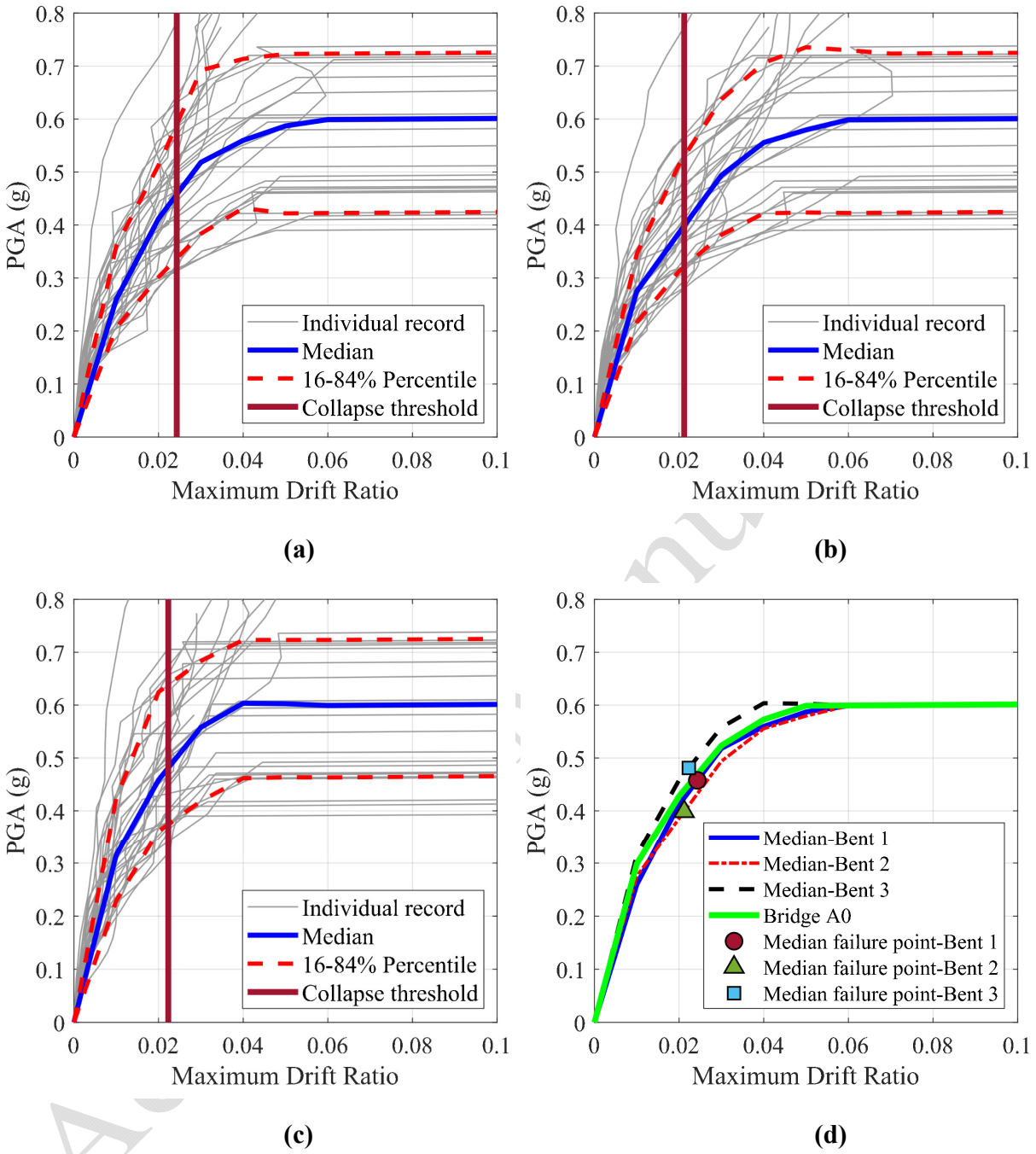

Fig. 15. IDA results of bridge C1: (a) response of tall bent (bent 1); (b) response of short bent (bent 2); (c) response of medium-height bent (bent 3), and (d) median response of all bents

Fig. 16 shows an exemplary base shear-drift ratio response of all bents of bridge C1 subject to Hector Mine ground motion at PGA=0.4g. Same to Figs. 12 and 14, this record and IM were

selected to represent the median dynamic cyclic behaviour of the critical bent (here bent 2) at the median IM. Fig.16 clearly shows the higher drift ratio and lateral seismic force of bent 2 than other bents. This shows the higher vulnerability of shorter columns in bridge C1 and confirms the results provided in Fig.15 (d).

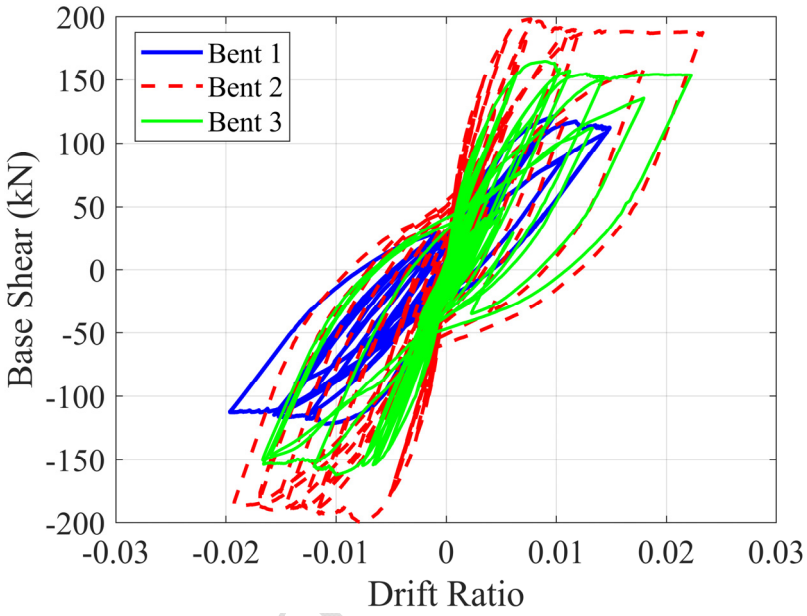

Fig. 16. An exemplary hysteretic response of individual bents of bridge C1 under Hector Mine ground motion

6.2.2 IDA Results at the Material Level

The results presented in the previous section, which were in terms of the global structural response, indicated that irregular bridges with varied layouts show different seismic behaviour and failure sequences of bents. However, the global response of structural components cannot provide sufficient information on the material scale to explain such differences. Hence, the response of core concrete at the critical regions of all bridge columns is recorded during the IDAs. Then, the peak compressive strain of core concrete at each IM level is normalised by its corresponding

ultimate value ε_{cu} (Eq. (1)). This way, the normalised core concrete strain will be between zero and unity, where the latter corresponds to the onset of concrete failure.

Fig. 17 shows the variation of normalised core concrete response versus the input levels of IM in each bent of bridge A1. As shown in Figs. 17(a-c), the corresponding IMs to the onset of concrete failure are highly scattered. This shows that the failure of bents at the material scale is highly dependent on the characteristics of the input ground motions. For instance, as shown in Fig. 17(b), the associated IMs with the onset of concrete failure in the critical section of bent 2 varies from approximately 0.4g to 1g. Fig. 17(d) compares the median response of concrete in the columns of bent 1, bent 2, and bent 3. This figure shows that the onset of concrete failure of bent 1 occurs earlier at approximately PGA=0.4g. Then, it took place in sequence in bent 2 and bent 3. This conclusion is in line with those discussed in the previous section.

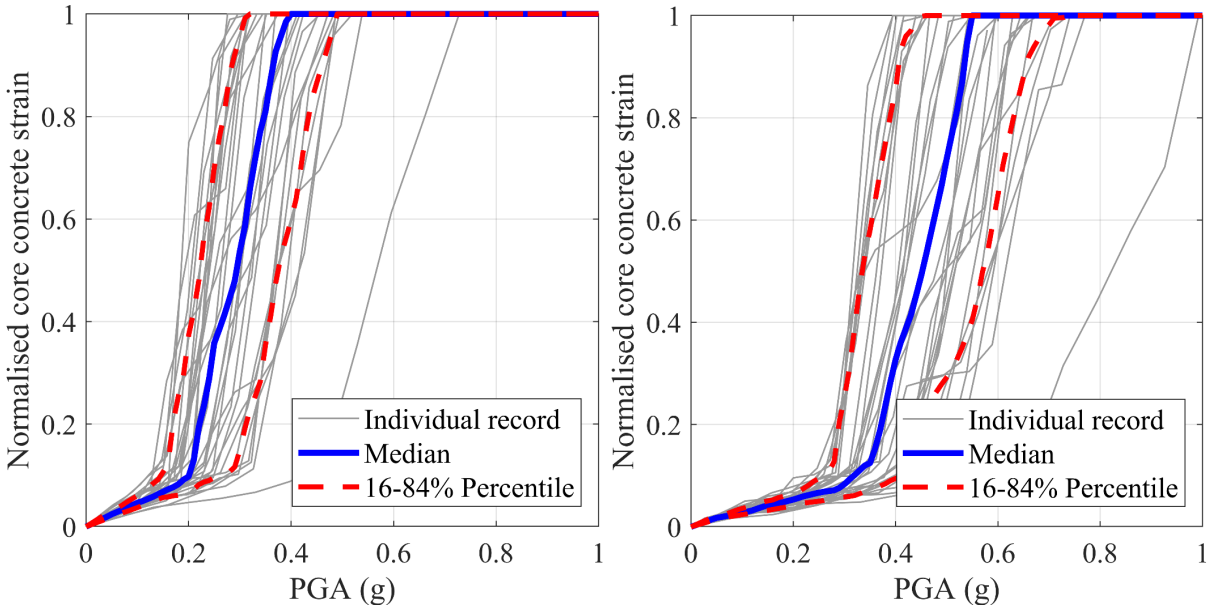

(a) **(b)**

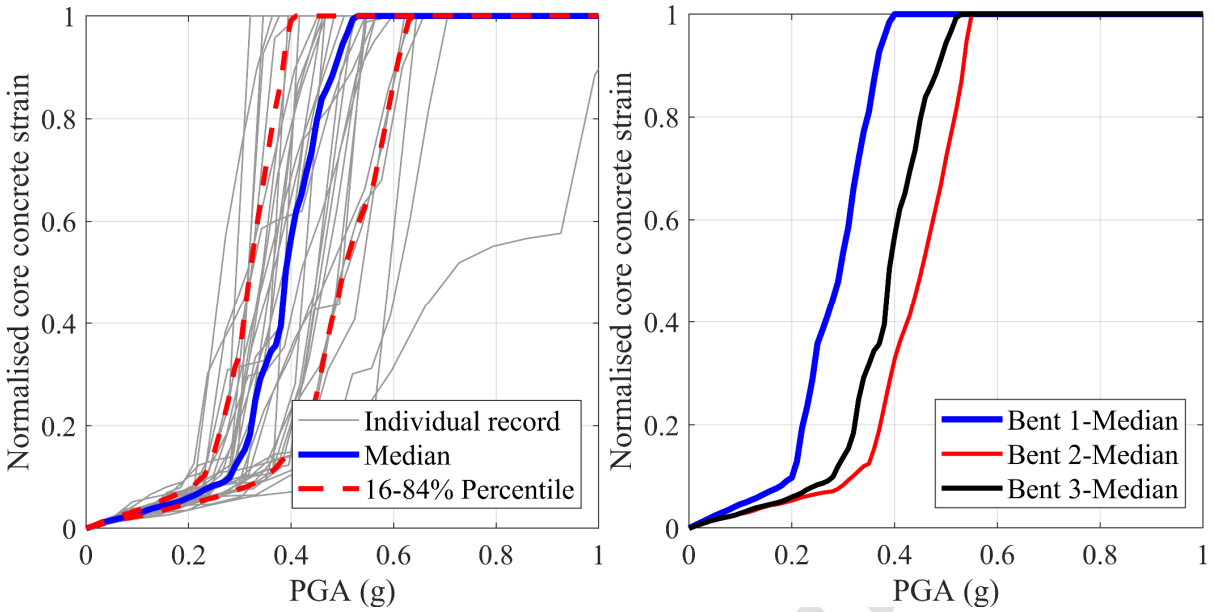

(c) **(d)**

Fig. 17. The normalised response of core concrete at the base of columns in bridge A1: (a) bent 1; (b) bent 2; (c) bent 3, and (d) median responses

Similarly, in Figs. (18-19) the variation of normalised concrete strains is plotted against the input IMs for different bents of bridge B1 and bridge C1. The median response of core concrete given in these figures (Fig. 18(d) and Fig. 19(d)) confirm the predicted failure sequence of columns in bridges B1 and C1. For instance, Fig. 18(d) shows that the onset of concrete failure reaches earlier in taller columns of bridge B1 (located in bent 1), approximately at PGA= 0.42g. This is in agreement with the results discussed in Fig. 13(d) for the same bridge.

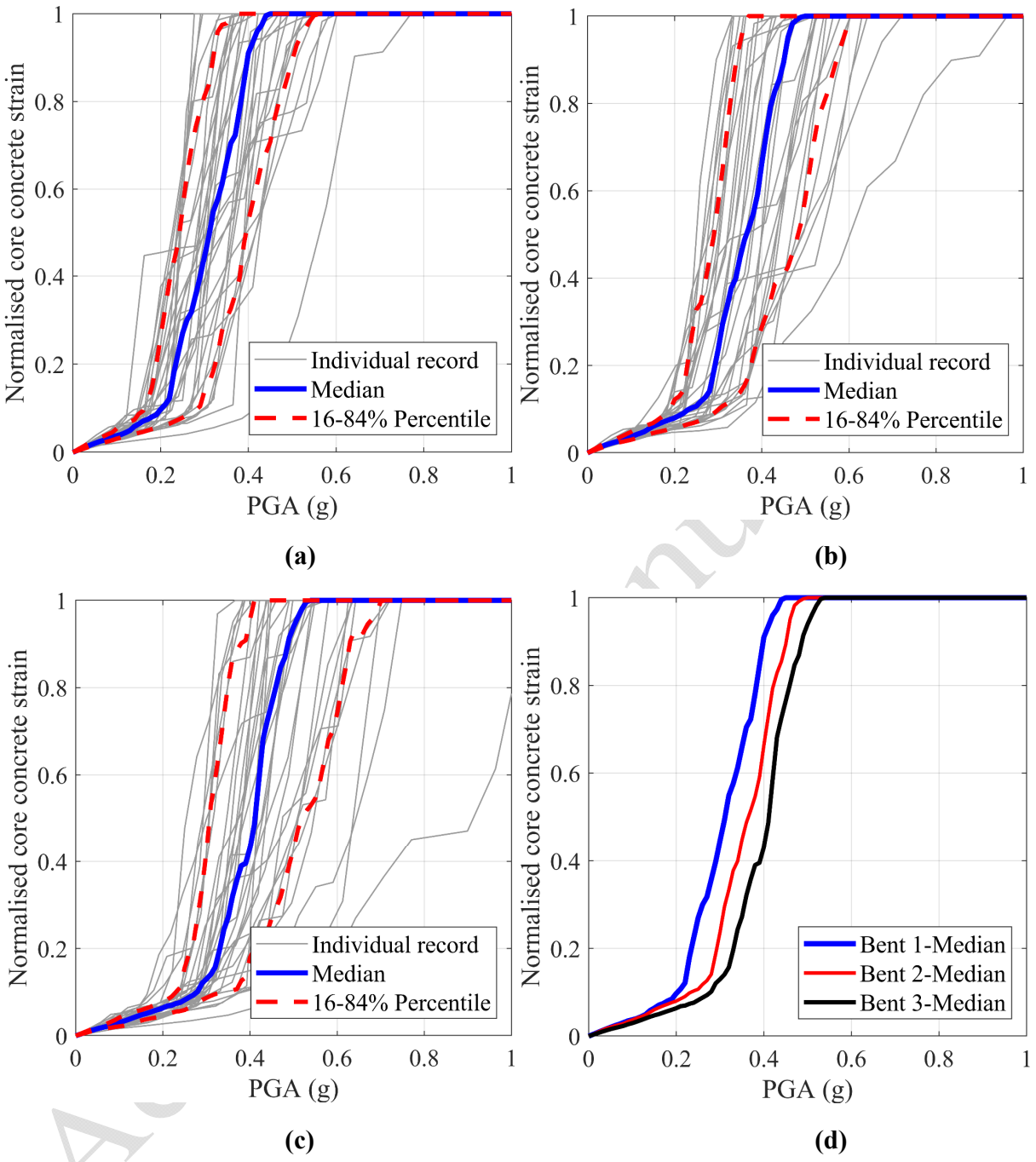

Fig. 18. The normalised response of core concrete at the base of columns in bridge B1: (a) bent 1; (b) bent 2; (c) bent 3, and (d) median responses

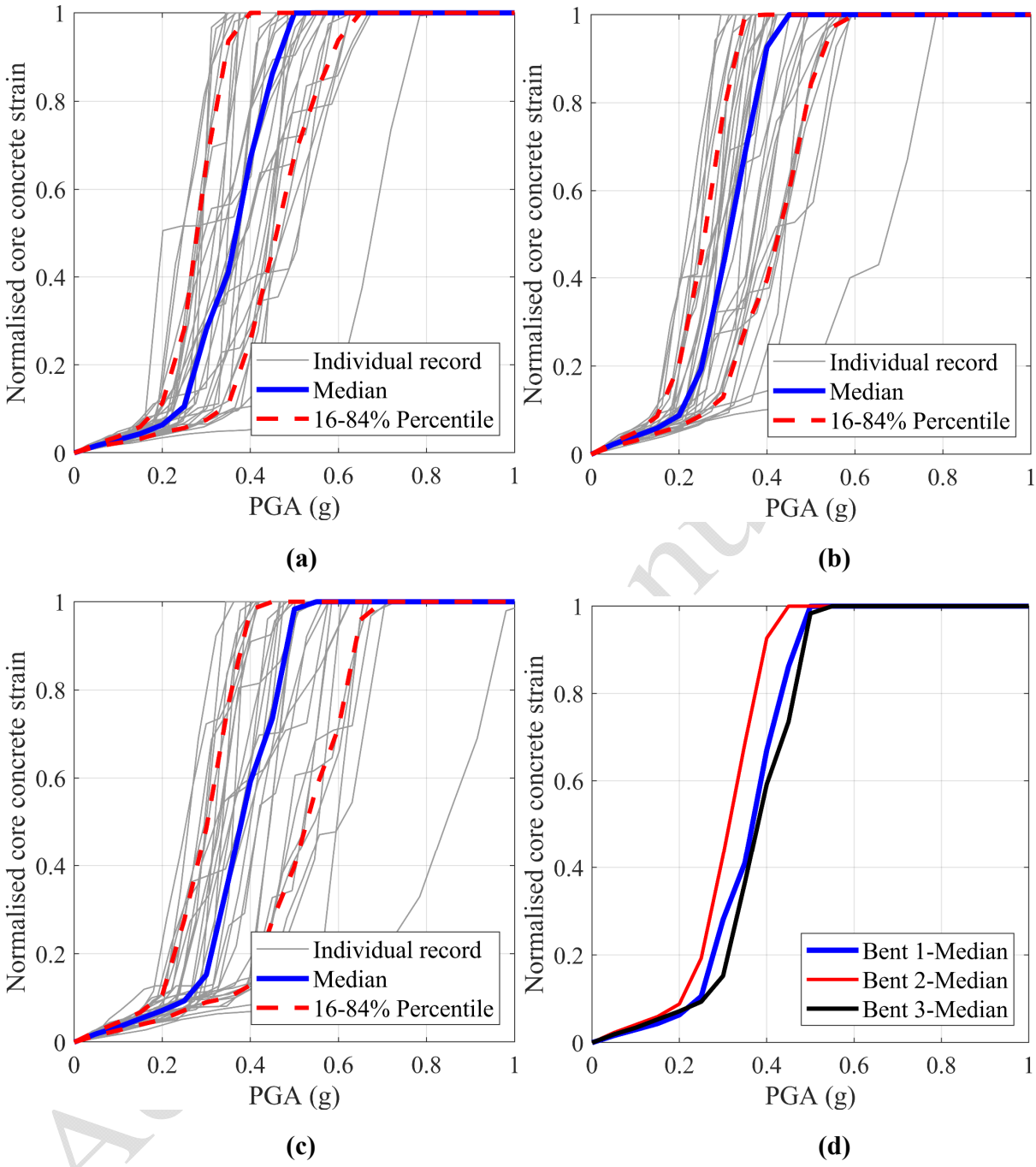

Fig. 19. The normalised response of core concrete at the base of columns in bridge C1: (a) bent 1; (b) bent 2; (c) bent 3, and (d) median responses

6.3 Analysis Results of Bridges A2, B2, and C2

The previous section showed the influence of triggered unbalanced demands due to the unequal stiffness of the piers on nonlinear dynamic performance and failure sequence of bridges A1, B1 and C1. However, as shown in Fig. 1, the configuration of super-imposed masses placed on the deck also induces unbalanced inertia forces on each bent. This is because, the amount of allocated masses on bent 1 and bent 3 is significantly greater than that of bent 2. This raises a question: Which source causes much unbalanced seismic behaviour in an irregular multi-span RC bridge: stiffness irregularity, or unequal distribution of gravity masses along the length of the bridge superstructure?

As listed in Table 1, three additional bridge types, including A2, B2 and C2 are considered to answer the above question. The only difference between these three cases with their corresponding original layouts (i.e. A1, B1 and C1 bridge types) is the equal distribution of super-imposed masses between all bridge piers, which translates to 13.5 tons on each column. Therefore, changing the distribution pattern of super-imposed masses, the IDAs are repeated for the A2, B2 and C2 bridge layouts.

Figs. 20(a), 20(b) and 20(c) present the median IDA results of bridges A2, B2 and C2, respectively. A simple comparison between these results with those given in Figs. 11(d), 13(d) and 15(d), show that the summarised IDA curves of bridges A2, B2 and C2 are approximately the same as those of bridges A1, B1 and C1, respectively. Moreover, the failure sequence of different bents is not affected by the equal distribution of masses (Figs. 20 (a-c)). The only noteworthy change is the slightly higher median IM associated with the onset of failure of bent 1 and bent 3 in all the equally distributed mass bridge cases compared to their corresponding IM in bridges A1, B1 and C1. For

instance, while in bridge B1 the associated median IM with the collapse of bent 3 is approximately PGA=0.45g (Fig. 13(d)); the corresponding value of IM is increased in bridge B2 (Fig. 20(b)).

It can be concluded from the above discussion that, for the bridge layouts and ground motion set considered in this study, the equal/unequal distribution of super-imposed masses among the different bents has a negligible impact on the unbalanced seismic ductility demand of unequal height bridge piers. The reason for such results is that in the considered A2, B2 and C2 bridge layouts, the total amount of superstructure mass of the system is not changed, and it is just equally distributed among the columns. Moreover, the deck is rigid, and all the columns move with the deck together, and hence, the effect of mass distribution in comparison to the stiffness difference between the adjacent columns is negligible. Furthermore, considering the dynamic equation of motion, a slight change in the tributary mass on each bent doesn't significantly affect the overall system response. In conclusion, the irregular seismic response of considered bridges with non-uniform column heights stems mainly from the substructure stiffness irregularity.

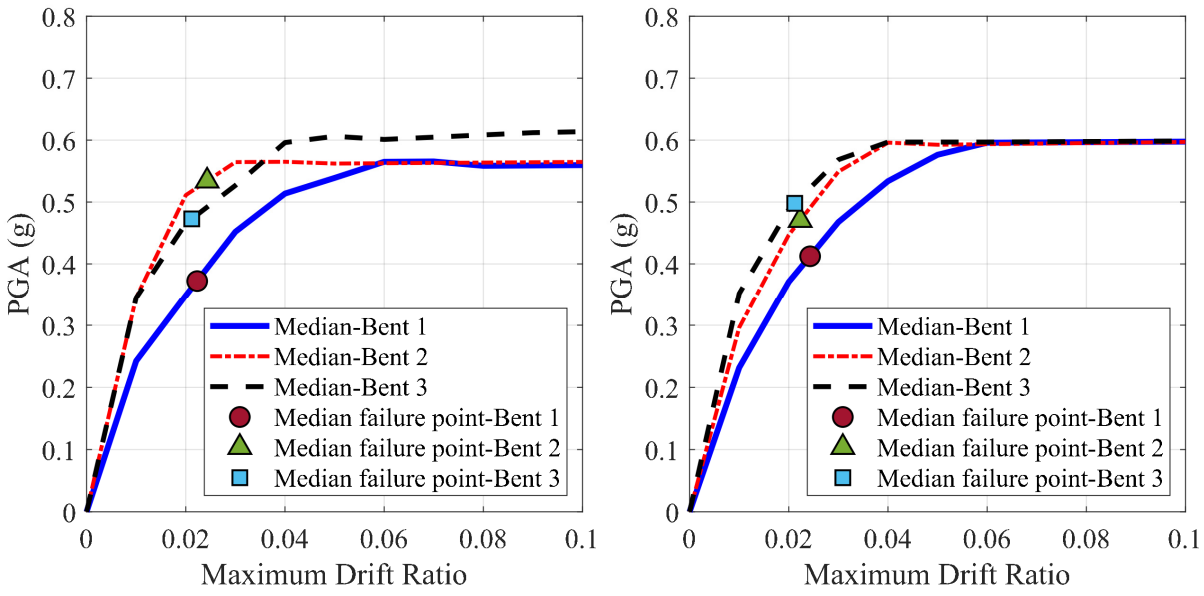

(a) **(b)**

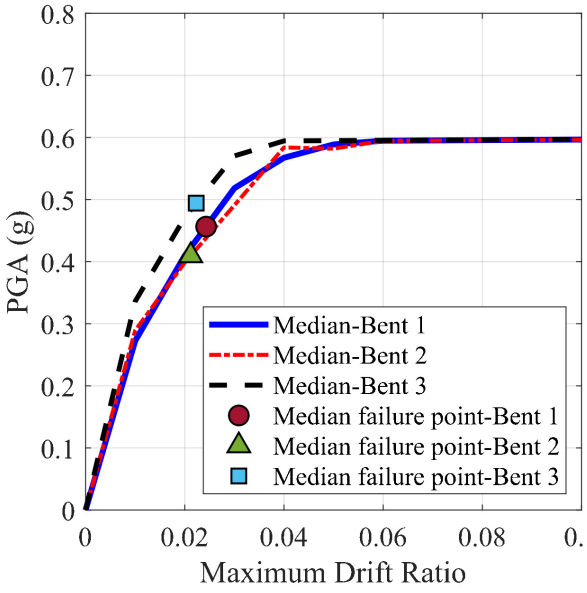

(c)

Fig. 20. Median IDA results of: (a) bridge A2; (b) bridge B2, and (c) bridge C2

7. Seismic Fragility Analysis

In this section, the failure probability of different bents is analysed using the seismic fragility curves of each bent. The fragility curves are developed using the following fragility function [46]:

$$P[EDP \geq DLS_i \mid PGA = x] = 1 - \Phi\left(\frac{\ln(DLS_i) - \ln(\theta)}{\beta}\right) \quad (2).$$

The left side of Eq. (2), is a conditional probability function that gives the exceedance probability of EDP from i^{th} Damage Limit State (DLS_i) given that PGA equals x. Moreover, $\Phi(.)$ is the lognormal distribution function with a logarithmic mean ($\ln(\theta)$), and logarithmic standard deviation (β) can be obtained from Eqs. (3-4), respectively:

$$\ln(\theta) = \frac{\sum_{i=1}^{n} \ln(EDP)}{n} \quad (3)$$

$$\beta = \sqrt{\frac{\sum_{i=1}^{n} \left(\ln(EDP) - \ln(\theta)\right)^2}{n-1}} \tag{4}$$

In order to plot seismic fragility curves of each bent, the associated drift ratio with the concrete crushing strain of each bent is extracted from the nonlinear pushover analysis results (as shown in Fig. 8) and considered as DLS_i in Eq. (2).

Fig. 21 presents the fragility curves of each bent in A1, B1 and C1 bridge layouts as well as the fragility curve of the reference bridge A0. Fig. 21(a) shows that, in bridge A1, the failure probability of bent 1 is higher than others. However, Fig. 21(b) shows that in bridge B1, taller piers are critical due to the higher probability of failure for any hazard levels. Conversely, in this height arrangement of piers, short piers have the most negligible collapse probability among the other piers. Finally, Fig. 21(c) indicates that shorter piers are more vulnerable than others in bridge C1. For example, for PGA=0.5g, the failure probability of bent 1, bent 2 and bent 3 are approximately 60%, 75%, and 50%, respectively.

Furthermore, Fig. 21 shows that the regular bridge is less fragile than the failure governing bents of selected irregular bridges. For instance, under PGA=0.4g, the failure probability of bent 1 of bridge A1 is approximately 37% higher than bridge A0 (Fig. 21(a)). However, the difference between the failure probability of studied regular and irregular bridges varies for the alternative height arrangement of unequal-height piers. For example, under PGA=0.4g, the difference between the failure probability of bent 1 of bridge B1 and that of bridge A0 is about 16% (Fig. 21(b)).

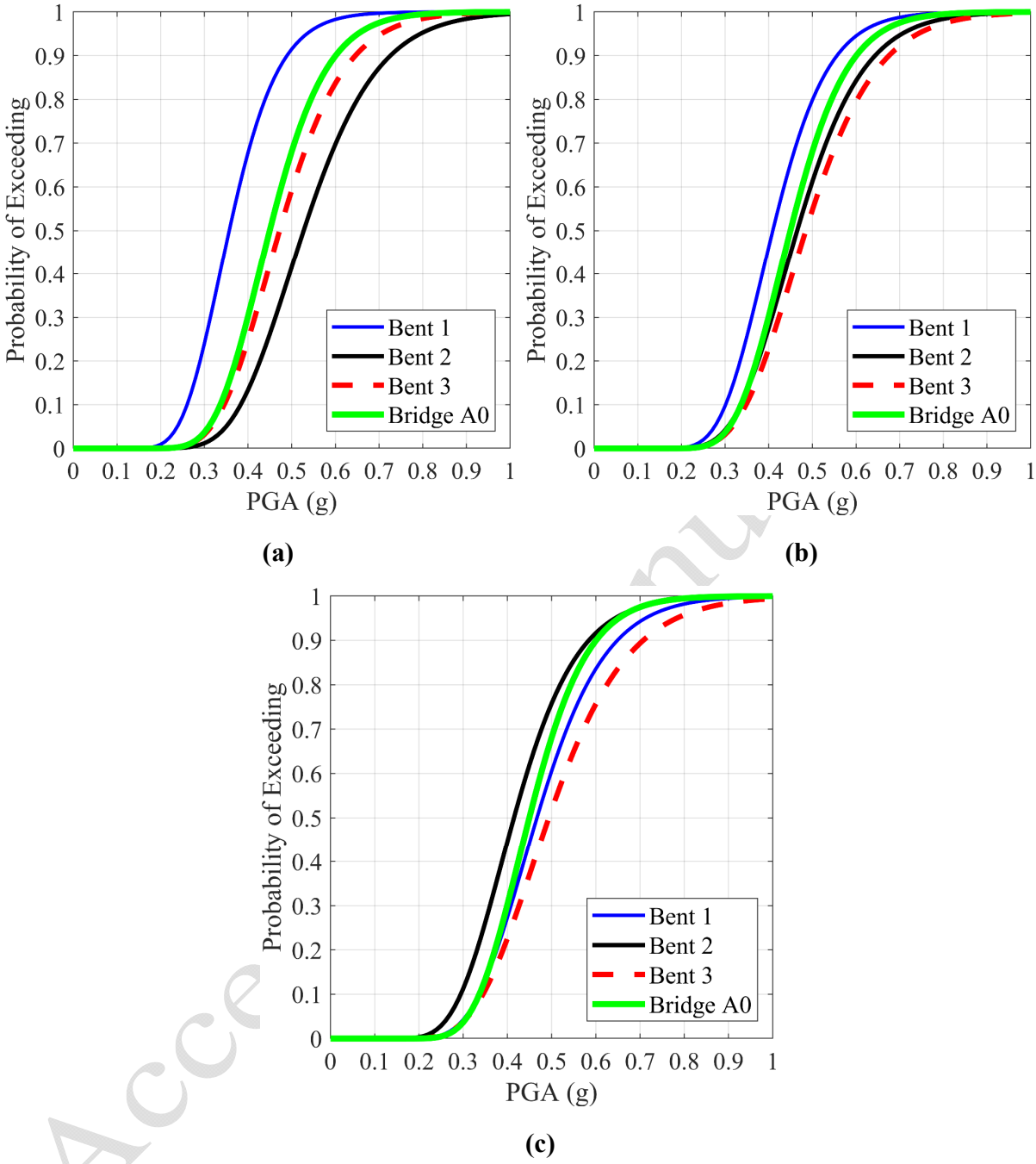

Fig. 21. Developed fragility curves: (a) bridge A1; (b) bridge B1, and (c) bridge C1

To investigate the influence of bridge layout on the vulnerability of piers of the same height, in Fig. 22, the fragility curves of short, medium and tall bents are compared. Fig. 22(a) shows that the vulnerability of shorter piers is greater in C1 layout, where these piers are placed in the intermediate of taller and medium height piers.

Fig. 22(b) compares the vulnerability of medium-height piers in hypothetical A1, B1 and C1 bridge layouts. The fragility curve of bridge A0 is also presented in this figure as all the piers of this bridge are the same height as those of medium-height piers in A1, B1 and C1 bridges. As can be seen in this figure, the probability of collapse of these piers is significantly higher in A1 layout. For instance, the failure probability of medium-height piers is higher than 90% in A1 layout, whereas it is about 60%, and 50% for B1 and C1 layouts, respectively. Moreover, Fig. 22(b) shows that, while the failure probability of regular bridge (bridge A0) for a given earthquake intensity level is lesser than bridge A1; it is higher than that of bridges B1 and C1. This is because, as discussed earlier in Section 6.2, unlike bridge A1, the failure of bridges B1 and C1 is not governed by the medium-height piers. Finally, Fig 22(c) shows that the taller piers are more vulnerable in B1 layout. Oppositely, these piers are less vulnerable in A1 layout.

The above discussion confirms that the bridge layout significantly influences the vulnerability of piers of varying heights.

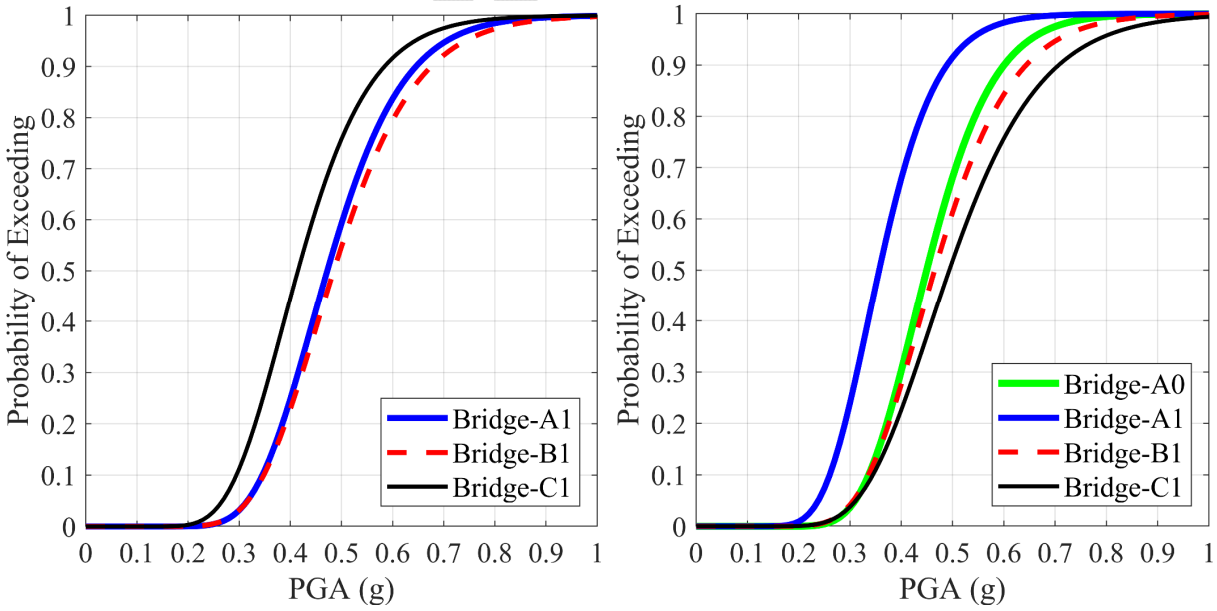

(a) **(b)**

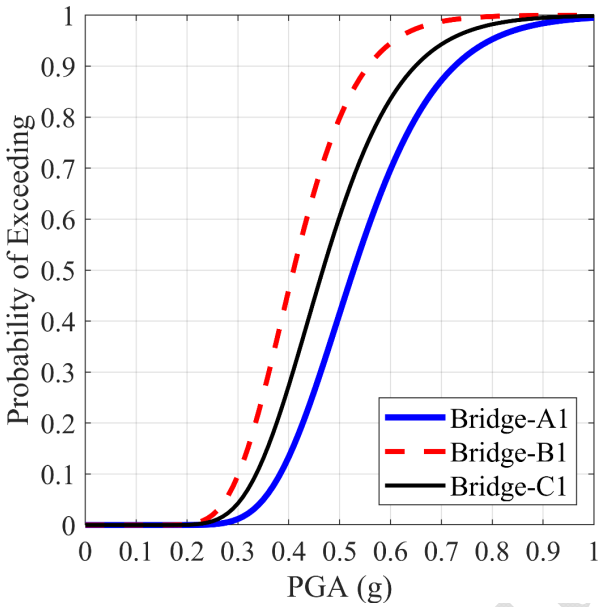

(c)

Fig. 22. Comparing the failure probability of piers of varying height in the studied bridges: (a) short piers; (b) medium height piers, and (c) tall piers

8. Conclusions

This paper investigated the seismic performance and fragility of multi-span RC bridges with unequal pier heights located in the mountainous areas, where the practical considerations dictate constructing such bridges. An advanced three-dimensional finite element model was developed in OpenSees to simulate the nonlinear seismic behaviour of the multi-span RC bridges with stiffness irregularity. The model was successfully validated by the large-scale shake table test results of a benchmark two-span irregular RC bridge specimen available in the literature. Elastic modal analysis, nonlinear pushover analysis, IDA and fragility analysis were carried out on six different irregular layouts of the benchmark bridge specimen to investigate the complex seismic behaviour of irregular RC bridges with varying height arrangements of piers. Moreover, the influence of equal/unequal distribution of inertia forces due to the equal/unequal tributary super-imposed

masses between different piers of the studied bridges is investigated and discussed. The following conclusions can be drawn from the findings of this paper:

- The modal periods and mass participation of higher modes of the reference two-span irregular RC bridge significantly depend on the height arrangement of piers. For instance, while the predominant vibration mode of bridge A1 is in its longitudinal direction, the primary mode of vibration of bridge B1 and bridge C1 is in the transverse direction. Moreover, while the mass participation of predominant transverse mode in bridge A1 is approximately 79%, the highest mass participation in bridge C1 belongs to the second primary transverse mode by about 66%.
- In the studied irregular RC bridges, the failure sequence of piers of varying heights crucially depends on the height arrangements of bents. For instance, the medium-height bent is critical and fails earlier than other bents in the medium-tall-short arrangement of bents (bridge A1). However, in a tall-medium-short arrangement of bents (bridge B1), the tallest piers become critical and fail before the other piers in lower earthquake intensity levels. Alternatively, short piers are critical members in the tall-short-medium height arrangement of piers (bridge C1).
- The equal/unequal distribution of super-imposed masses among the bents of varying heights slightly affects the median IM at their failure. However, it has less influence on the unbalanced seismic ductility demand and failure sequence of unequal height bridge piers than the substructure stiffness irregularity.
- The bridge layout significantly influences the vulnerability of piers of varying heights. Therefore, the typical presumption on a higher failure probability of shorter piers due to their higher seismic force absorption might be misleading. This conclusion could influence

future studies on balanced design procedures or damage mitigation methodologies (connection isolation, using damper devices, etc.) for irregular multi-span RC bridges.

CRediT author statement

Ebrahim Afsar Dizaj: Writing original draft, Methodology, Conceptualization, Finite Element Modelling, Validation, Formal Analysis. **Mohammad Reza Salami:** Methodology, Investigation, Visualization, Modal Analysis, Review & Editing, Resources. **Mohammad Mehdi Kashani:** Supervision, Review & Editing, Visualization.

Declaration of Competing Interest

The authors declare that they have no known competing financial interests or personal relationships that could have appeared to influence the work reported in this paper.

References

1. Ryall MJ. Bridge Management. Second Edition, 2009. ISBN 978-0-7506-8511-5.

2. Kappos AJ, Manolis GD, Moschonas IF. Seismic assessment and design of R/C bridges with irregular configuration, including SSI effects. Eng Struct 2002; 24(10): 1337–1348. https://doi.org/10.1016/S0141-0296(02)00068-8.

3. Guirguis JEB, Mehanny SSF. Evaluating code criteria for regular seismic behavior of continuous concrete box girder bridges with unequal height piers. J Bridge Eng 2013; 18(6):486–498. DOI: 10.1061/(ASCE)BE.1943-5592.0000383.

4. Priestley MJN, Seible F, Calvi GM. Seismic design and retrofit of bridges. Hoboken, NJ, USA: John Wiley & Sons, Inc; 1996.

5. Sajed M, and Tehrani P. Effects of column and superstructure irregularity on the seismic response of four-span RC bridges. Structures, 2020: 28: 1400-1412. https://doi.org/10.1016/j.istruc.2020.09.057.

6. Akbari R. Cyclic response of RC continuous span bridges with irregular configuration in longitudinal direction. J Struct Infrastruct Engineering 2013; 9(2): 161–171. https://doi.org/10.1080/15732479.2010.510528.

7. Isakovi´ c T, Fischinger M. Higher modes in simplified inelastic seismic analysis of single column bent viaducts. J Earthquake Eng Struct Dyn 2006; 35(1): 95–114. https://doi.org/10.1002/eqe.535.

8. Tamanani M, Gian Y, Ayoub A. Evaluation of code criteria for bridges with unequal pier heights. Bull Earthq Eng 2016; 14(11): 3151–3174. https://doi.org/10.1007/s10518-016-9941-4.

9. AASHTO. AASHTO Guide Specifications for LRFD Seismic Bridge Design. Washington: American Association of State Highway and Transportation Officials; 2011.

10. Caltrans. Caltrans Seismic Design Criteria-Version 1.7. Sacramento, California: California Department of Transportation; 2013.

11. Priestley, M. J. N. The need for displacement-based design and analysis. Advanced earthquake engineering analysis, 2007, Vol. 494, CISM International Center for Mechanical Sciences, Springer, Vienna, Austria, 121–132.

12. Xiang N, Li J. Utilizing yielding steel dampers to mitigate transverse seismic irregularity of a multispan continuous bridge with unequal height piers. Engineering Structures, 2020; 110056, https://doi.org/10.1016/j.engstruct.2019.110056.

13. Ishac MG, Mehanny SSF. Do mixed pier-to-deck connections alleviate irregularity of seismic response of bridges with unequal height piers? Bull Earthq Eng 2017; 15(1): 97–121. https://doi.org/10.1007/s10518-016-9958-8.

14. Jara JM, Villanueva, D, Jara M, Olmos BA. Isolation parameters for improving the seismic performance of irregular bridges. Bull Earthq Eng. 2013; 11: 663–686.

https://doi.org/10.1007/s10518-012-9398-z.

15. Soleimani F, Vidakovic B, DesRoches R, Padgett J. Identification of the significant uncertain parameters in the seismic response of irregular bridges. J Eng Struct 2017; 141: 356–372. http://dx.doi.org/10.1016/j.engstruct.2017.03.017.

16. Soltanieh S, Memarpour MM, Kilanehei F. Performance assessment of bridge-soil-foundation system with irregular configuration considering ground motion directionality effects. Soil Dyn Earthq Eng 2019; 118: 19–34. https://doi.org/10.1016/j.soildyn.2018.11.006.

17. Hu Y, and Guo W. Seismic response of high-speed railway bridge-track system considering unequal-height pier configurations. Soil Dynamics and Earthquake Engineering, 2020; 137: 106250. https://doi.org/10.1016/j.soildyn.2020.106250.

18. Abbasi M, Zakeri B, Amiri GG. Probabilistic seismic assessment of multiframe concrete box-girder bridges with unequal-height piers. J Perform Constr Facil 2015; 04015016. DOI: 10.1061/(ASCE)CF.1943-5509.0000753.

19. Jara JM, Reynoso JR, Olmos BA, Jara M. Expected seismic performance of irregular medium-span simply supported bridges on soft and hard soils. Eng Struct 2015; 98:174–185. https://doi.org/10.1016/j.engstruct.2015.04.032.

20. Saiidi MS, Vosooghi A, Nelson RB. Shake-table studies of a four-span reinforced concrete bridge. J Struct Eng 2012; 139(8): 1352–1361. https://doi.org/10.1061/(ASCE)ST.1943-541X.0000790.

21. Kaleybar RS, Tehrani P. Investigating seismic behavior of horizontally curved RC bridges with different types of irregularity in comparison with equivalent straight bridges. Structures, 2021; 33: 2570-2586. https://doi.org/10.1016/j.istruc.2021.06.014.

22. Camacho VT, Lopes M and Oliveira CS. Multivariate analysis of regular and irregular RC bridges and characterization of earthquake behaviour according to stiffness-based indexes. Bull Earthquake Eng, 2022; 20: 415–448. https://doi.org/10.1007/s10518-021-01223-9.

23. Jara JM, Jara M, Hernández H, Olmos BA. Use of sliding multirotational devices of an irregular bridge in a zone of high seismicity. KSCE J Civ Eng 2013; 17: 122–132. https://doi.org/10.1007/s12205-013-1063-9.

24. Gómez-Soberón MC, Pérez E, Salas D, and León-Escobedo DD. Seismic vulnerability through drift assessment for bridges with geometrical irregularities. European Journal of Environmental and Civil Engineering, 2019. https://doi.org/10.1080/19648189.2019.1686428.

25. Noori HZ, Amiri GG, Nekooei M, Zakeri B. Seismic fragility assessment of skewed MSSSI girder concrete bridges with unequal height columns. J Earthq Tsunami 2016; 10(01): 1550013. https://doi.org/10.1142/S179343111550013X.

26. Akbari R. Seismic fragility analysis of reinforced concrete continuous span bridges with irregular configuration. Struct Infrastruct Eng 2012; 8: 873–889. https://doi.org/10.1080/15732471003653017.

27. Rezaei H, Arabestani S, Akbari R, and Farsangi EN. The effects of earthquake incidence angle on the seismic fragility of reinforced concrete box-girder bridges of unequal pier heights. Structure and Infrastructure Engineering. 2020; 18(2): 278-293. https://doi.org/10.1080/15732479.2020.1842467.

28. Mosleh A, Jara J, Razzaghi MS, and Varum H. Probabilistic seismic performance analysis of RC bridges. Journal of Earthquake Engineering, 2020, 24(11): 1704-1728. https://doi.org/10.1080/13632469.2018.1477637.

29. Rasouli M, Shirvand MR, and Ardakani RR. Performance-based design method for isolated hollow RC piers with irregularity in height. Structural Concrete, 2022, https://doi.org/10.1002/suco.202200083.

30. Akbari R, and Maalek S. A review on the seismic behaviour of irregular bridges. Proceedings of the Institution of Civil Engineers-Structures and Buildings, 2018; 171(7): 552-580.

31. McKenna F. OpenSees: A framework for earthquake engineering simulation. Computing in Science & Engineering. 2011; 13(4): 58–66. doi:10.1109/MCSE.2011.66.

32. Johnson N, Ranf RT, Saiidi MS, Sanders D, and Eberhard M. Seismic testing of a two-span reinforced concrete bridge. Journal of Bridge Engineering, 2008; 13(2): 173-182. https://doi.org/10.1061/(ASCE)1084-0702(2008)13:2(173).

33. Kashani MM, Lowes LN, Crewe AJ, and Alexander NA. Nonlinear fibre element modelling of RC bridge piers considering inelastic buckling of reinforcement. Engineering Structures, 2016; 116, 163–177. doi:10.1016/j.engstruct.2016.02.051.

34. Salami MR, Afsar Dizaj E, Kashani MM. The behavior of Rectangular and Circular Reinforced Concrete Columns under Biaxial Multiple Excitation. Computer Modeling in Engineering and Sciences, 2019; 120 (3): 677-691. DOI: 10.32604/cmes.2019.05666.

35. Salami MR, Afsar Dizaj E, Kashani MM. Fragility analysis of rectangular and circular reinforced concrete columns under bidirectional multiple excitations. Engineering Structures, 2021; 233: 111887. https://doi.org/10.1016/j.engstruct.2021.111887.

36. Zhao J, Sritharan S. Modeling of strain penetration effects in fiber-based analysis of reinforced concrete structures. ACI Structural Journal, 2007; 104(2): 133–141.

37. Dhakal RP, Maekawa K. Reinforcement stability and fracture of cover concrete in reinforced concrete members. J Struct Eng 2002; 128(10): 1253–1262. https://doi.org/10.1061/(ASCE)0733-9445(2002)128:10(1253).

38. Berry MP, and Eberhard MO. Performance modelling strategies for modern reinforced concrete bridge columns. PEER research report. Univ. of Calif, 67(11) Berkeley, 2006.

39. Mander JB, Priestley MJN, Park R. Observed stress–strain behavior of confined concrete. J Struct Eng 1988; 114(8): 1827–1849. https://doi.org/10.1061/(ASCE)0733-9445(1988)114:8(1827).

40. Kashani MM, Lowes LN, Crewe AJ, and Alexander NA. Phenomenological hysteretic model for corroded reinforcing bars including inelastic buckling and low-cycle fatigue degradation. Computers and Structures, 2015; 156: 58–71. https://doi.org/10.1016/j.compstruc.2015.04.005.

41. Dizaj EA, Madandoust R, Kashani MM. Probabilistic seismic vulnerability analysis of corroded reinforced concrete frames including spatial variability of pitting corrosion. Soil Dyn Earthq Eng 2018; 114: 97–112. https://doi.org/10.1016/j.soildyn.2018.07.013.

42. Afsar Dizaj E, Kashani MM. Nonlinear Structural Performance and Seismic Fragility of Corroded Reinforced Concrete Structures: Modelling Guidelines. European Journal of Environmental and Civil Engineering, 2021. https://doi.org/10.1080/19648189.2021.1896582.

43. Priestley M, and Paulay T. Seismic design of reinforced concrete and masonry buildings. New York: John Wiley & Sons, Inc, 1992.

44. Vamvatsikos D, and Cornell CA. Incremental dynamic analysis. Earthquake Engineering and Structural Dynamics, 2002; 31(3): 491–514. doi:10.1002/eqe.141.

45. FEMA P695. Quantification of building seismic performance factors. Federal Emergency Management Agency, Washington, DC, 2009.

46. Afsar Dizaj E, Salami MR, and Kashani MM. Seismic vulnerability assessment of ageing reinforced concrete structures under real mainshock-aftershock ground motions. Structure and Infrastructure Engineering, 2021. https://doi.org/10.1080/15732479.2021.1919148.